Phase Separation and Cytotoxicity of Tau are Modulated by Protein Disulfide Isomerase and S-nitrosylation of this Molecular Chaperone

Kan Wang[1,†], Jia-Qi Liu[1,†], Tao Zhong[1], Xiao-Ling Liu[1], Yan Zeng[1], Xinhua Qiao[2], Ting Xie[2], Yuzhe Chen[2], Ying-Ying Gao[1], Bo Tang[3], Jia Li[4], Jun Zhou[4], Dai-Wen Pang[3], Jie Chen[1], Chang Chen[2] and Yi Liang[1]

*1 - **Hubei Key Laboratory of Cell Homeostasis,** College of Life Sciences, Wuhan University, Wuhan 430072, China*
*2 - **National Laboratory of Biomacromolecules,** CAS Center for Excellence in Biomacromolecules, Institute of Biophysics, Chinese Academy of Sciences, Beijing 100101, China*
*3 - **Key Laboratory of Analytical Chemistry for Biology and Medicine (Ministry of Education),** College of Chemistry and Molecular Sciences, Wuhan University, Wuhan 430072, China*
*4 - **Hubei Key Laboratory of Bioinorganic Chemistry and Materia Medica,** School of Chemistry and Chemical Engineering, Huazhong University of Science and Technology, Wuhan 430074, China*

***Correspondence to Yi Liang:** liangyi@whu.edu.cn*
https://doi.org/10.1016/j.jmb.2020.02.013
Edited by Louise C. Serpell

Abstract

Cells have evolved molecular chaperones that modulate phase separation and misfolding of amyloidogenic proteins to prevent neurodegenerative diseases. Protein disulfide isomerase (PDI), mainly located at the endoplasmic reticulum and also present in the cytosol, acts as both an enzyme and a molecular chaperone. PDI is observed to be S-nitrosylated in the brain of Alzheimer's disease patients, but the mechanism has remained elusive. We herein report that both wild-type PDI and its quadruple cysteine mutant only having chaperone activity, significantly inhibit pathological phosphorylation and abnormal aggregation of Tau in cells, and significantly decrease the mitochondrial damage and Tau cytotoxicity resulting from Tau aberrant aggregation, highlighting the chaperone property of PDI. More importantly, we show that wild-type PDI is selectively recruited by liquid droplets of Tau, which significantly inhibits phase separation and stress granule formation of Tau, whereas S-nitrosylation of PDI abrogates the recruitment and inhibition. These findings demonstrate how phase separation of Tau is physiologically regulated by PDI and how S-nitrosylation of PDI, a perturbation in this regulation, leads to disease.

Introduction

Tau is an intrinsically disordered protein in neurons, whose major physiological function is the stabilization of neuronal microtubules through its microtubule-binding region $Tau_{244-372}$ [1–6]. Under physiological conditions, Tau keeps a balance between the microtubule-associated form and the free form, but under pathological conditions, it detaches from microtubules and aggregates into intracellular inclusions, such as neurofibrillary tangles (NFTs) in the brain of patients with Alzheimer's disease (AD) and related neurodegenerative diseases [2–9].

Liquid-liquid phase separation by natively unstructured proteins, such as Tau, or by proteins with low-complexity domains, such as fused in sarcoma (FUS), is the first step of protein aggregation, followed by a transition from liquid to solid phase, which generates membraneless organelles like stress granules and drives pathological fibril formation, which are critical events functionally linked to neurodegenerative diseases [10–25]. Recently, Tau has been reported to undergo liquid-liquid phase separation and form stress granules [24–35]. There

are several factors that affect the phase separation of Tau. These factors include those of the Tau protein itself, such as alternative splicing [26], phosphorylation [24,26,27], acetylation [28–30], and electrostatic interactions [24–28,31,32], and environmental factors, such as crowding agents [24–33] and polyanionic cofactors, including heparin and RNA [24,26–32].

Cells have evolved molecular chaperones as quality control proteins that modulate liquid-liquid phase separation and aggregation of amyloidogenic proteins to prevent neurodegenerative diseases [20–23,36–43]. Recently, three groups have reported in the same issue of *Cell* that Transportin 1, acting as a molecular chaperone, significantly inhibits the phase separation, stress granule formation and fibrillization of FUS [21–23]. The Alberti laboratory has demonstrated that Hsp70, a typical chaperone, plays a crucial role in hindering the formation of stress granules containing misfolded SOD1 [20] and that the HspB8-BAG3-Hsp70 chaperone complex prevents defective ribosomal product accumulation in stress granules [43]. Protein disulfide isomerase (PDI), a multifunctional protein mainly located at the endoplasmic reticulum (ER) of cells, acts as both an enzyme that catalyzes the formation, breakage, and rearrangement of protein disulfide bonds by two catalytic domains a and a' of PDI, and a redox-regulated chaperone that interacts with various substrates using a large hydrophobic pocket embedded in domain b' of PDI [44–49]. PDI is known to be present in the cytosol, as well as other locations [47,48,50–53]. Furthermore, a recent study shows that PDI translocates into the cytosol via an ER stress-induced protein reflux system [54]. PDI is found to be associated with numerous neurodegenerative diseases, most notably Alzheimer's, and believed to eliminate the neurotoxicity associated with ER stress and protein aggregation [50–53]. PDI is observed to be aberrantly S-nitrosylated in the brain of patients with AD or Parkinson's disease [50,52] and in spinal cords of patients with amyotrophic lateral sclerosis [51], but the mechanism behind this phenomenon has remained elusive. It also remains unknown how chaperones physiologically regulate Tau phase separation and toxicity in neuronal cells and how PDI modulates liquid-liquid de-mixing and stress granule association of proteins.

Here, we show that PDI plays a crucial role in preventing hyperphosphorylation and aggregation of Tau and decreasing mitochondrial dysfunction and Tau toxicity in cells. We demonstrate that PDI, which directly interacts with Tau in cells, acts as a Tau chaperone and suppresses liquid-liquid phase separation and stress granule association of Tau, but S-nitrosylation of PDI antagonizes this inhibitory effect. These findings reveal the molecular basis for a protective function of PDI in Tau phase separation and cytotoxicity, which could be exploited to develop therapeutic strategies against AD and other tauopathies.

Results

PDI directly interacts with Tau in cells

PDI and Tau proteins are observed to colocalize in NFTs in the hippocampus of AD brain [52,53]. However, it remains unclear where (in which organelle) PDI interacts with Tau in cells. The HEK-293T cell line was chosen because it is able to express high levels of fusion proteins and is very sensitive to the treatment of Tau oligomers or sodium arsenite. Bimolecular fluorescence complementation (BiFC) assay [55–57] was used to detect the scenario of Tau-PDI interaction in living HEK-293T cells. Enhanced green fluorescence protein (EGFP) was split into two nonfluorescent halves. The following Tau-PDI constructs were used in our BiFC assay, 2N4R Tau-$EGFP_{1\text{-}172}$ fusion protein (Fig. 1A) and signal peptide-HA-$EGFP_{155\text{-}238}$-a-b-b'-x-a'-c (PDI) fusion protein (Fig. 1B), that is, 2N4R Tau was fused to the N-terminal fragment of EGFP ($EGFP_{1\text{-}172}$), and the C-terminus of EGFP ($EGFP_{155\text{-}238}$) was inserted between the signal peptide and the amino acid coding sequence of PDI. HEK-293T cells transiently expressing both full-length Tau-$EGFP_{1\text{-}172}$ and $EGFP_{155\text{-}238}$-wild-type PDI or $EGFP_{155\text{-}238}$-dnPDI constructs were cultured for 1 day, then stained with ER Staining Kit (red, Fig. 1C and G), and visualized by confocal microscopy. Here, dominant-negative PDI (dnPDI) is a quadruple cysteine mutant C53A/C56A/C397A/C400A of PDI with both active sites mutated [50,58]. This stain is possibly not entirely ER specific. Specific interaction between Tau and wild-type PDI (Fig. 1C–F) or dnPDI (Fig. 1G–J) in the ER and the cytosol of living HEK-293T cells was detected by BiFC, and EGFP (green fluorescence) was clearly observed for these two specific interactions (Fig. 1D and H; Merge: Fig. 1E and I, light yellow tinged orange). This approach led to a surprising discovery that dnPDI, a mutant of PDI only having chaperone activity [50,58], also interacted with Tau in the ER and the cytosol of living cells (Fig. 1H). The following controls were used to validate the PDI-Tau interaction: HEK-293T cells transiently expressing both $EGFP_{1\text{-}172}$ and $EGFP_{155\text{-}238}$-PDI (Fig. S1I–L) or $EGFP_{155\text{-}238}$-dnPDI (Fig. S1A–D) or $EGFP_{155\text{-}238}$ (Fig. S1M–P) constructs or both full-length Tau-$EGFP_{1\text{-}172}$ and $EGFP_{155\text{-}238}$ constructs (Fig. S1E–H). EGFP (green) was not observed in these controls (Fig. S1B, 1F, 1J and 1N), indicating that no interactions between $EGFP_{1\text{-}172}$ and $EGFP_{155\text{-}238}$-dnPDI, between Tau-$EGFP_{1\text{-}172}$ and $EGFP_{155\text{-}238}$,

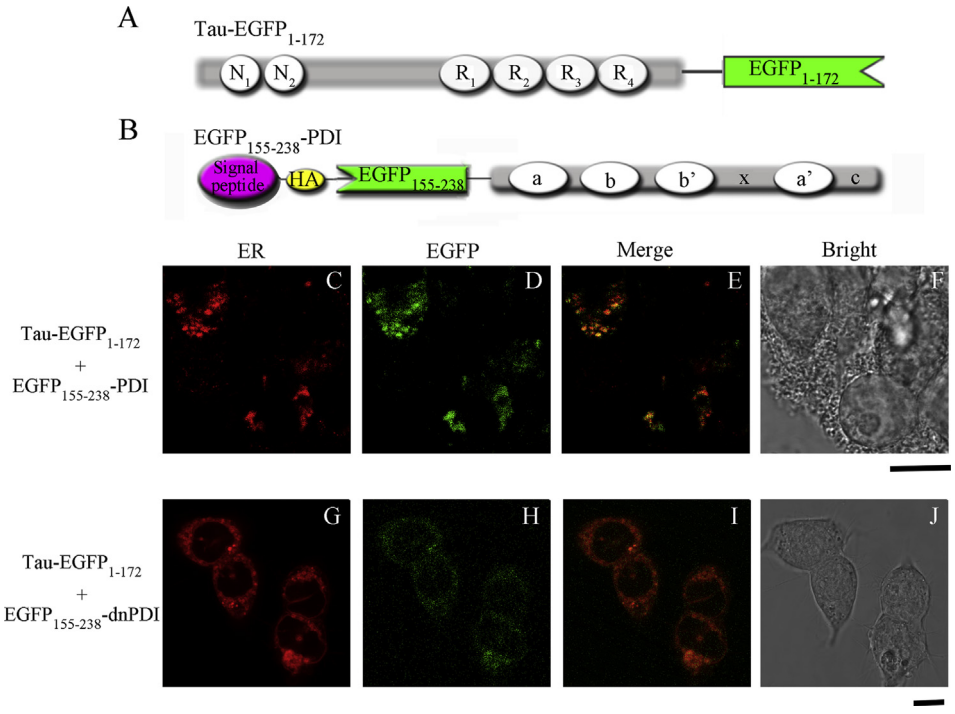

Fig. 1. Both wild-type PDI and its quadruple cysteine mutant interact with Tau in living cells. Schemes of Tau-PDI constructs used in BiFC assay: 2N4R Tau-EGFP$_{1\text{-}172}$ fusion protein (A) and signal peptide-HA-EGFP$_{155\text{-}238}$-a-b-b'-x-a'-c (PDI) fusion protein (B). Specific interaction between Tau and wild-type PDI (C–F) or dnPDI (G–J) in living cells was detected by BiFC. HEK-293T cells transiently expressing both full-length human Tau-EGFP$_{1\text{-}172}$ and signal peptide-HA-EGFP$_{155\text{-}238}$-PDI or signal peptide-HA-EGFP$_{155\text{-}238}$-dnPDI constructs were cultured for 1 day, then stained with ER Staining Kit (red, C and G), and visualized by confocal microscopy. EGFP (green fluorescence) was clearly observed in D and H (Merge: E and I, light yellow tinged orange). The scale bar represents 10 μm.

between EGFP$_{1\text{-}172}$ and EGFP$_{155\text{-}238}$-PDI, or between EGFP$_{1\text{-}172}$ and EGFP$_{155\text{-}238}$ in living cells were detected by BiFC. Because false positives are possible with BiFC assay, we then used other methods, such as coimmunoprecipitation (co-IP) assay to confirm this putative interaction. Our co-IP experiments visualized by the anti-Tau antibody Tau-5 and anti-HA antibody revealed that both wild-type PDI and dnPDI interact with Tau in HEK-293T cells (Fig. S2). Collectively, these data demonstrate that PDI and Tau are required for this putative interaction, and that both wild-type PDI and its quadruple cysteine mutant only having chaperone activity directly interact with Tau in cells.

PDI significantly inhibits Tau phosphorylation and aggregation in cells by acting as a chaperone

Because PDI directly interacts with Tau in cells, we wondered whether PDI might modulate Tau phosphorylation and aggregation in cells by acting as a chaperone. We, therefore, performed cell biological experiments in which Congo red, an anionic dye that is able to overcome the energy barrier for Tau aggregation and penetrate the cell membrane [59–61], was used as an agonist for Tau phosphorylation and aggregation in cells.

Because Tau phosphorylation at Ser-396 in the C-terminal region is one of the earliest events in AD and related neurodegenerative diseases [62,63], we first tested the hypothesis that PDI might act as a chaperone to regulate Tau phosphorylation at Ser-396 in cells. SH-SY5Y cells stably expressing full-length Tau or its pathogenic mutation ΔK280 (Fig. 2 and S3), cultured for 2 days, then transiently expressed HA-tagged wild-type PDI (Fig. 2F–J and S3F–J) or HA-tagged dnPDI (Fig. 2K–O and S3K–O) and incubated with 10 μM Congo red for 3 days, or directly incubated with 10 μM Congo red for 3 days (Fig. 2A–E and S3A–E), were immunostained with the anti-pS396 antibody (green) and anti-HA antibody (red), stained with 4',6-diamidino-2-phenylindole dihydrochloride (DAPI) (blue), and observed by confocal microscopy. ΔK280 of full-length Tau was chosen because it is able to cause typical AD or frontotemporal dementia pathology with corresponding NFTs [60,64–66]. Phosphorylation levels of full-length Tau and its pathogenic mutation ΔK280 at Ser-396 (green fluorescence) in

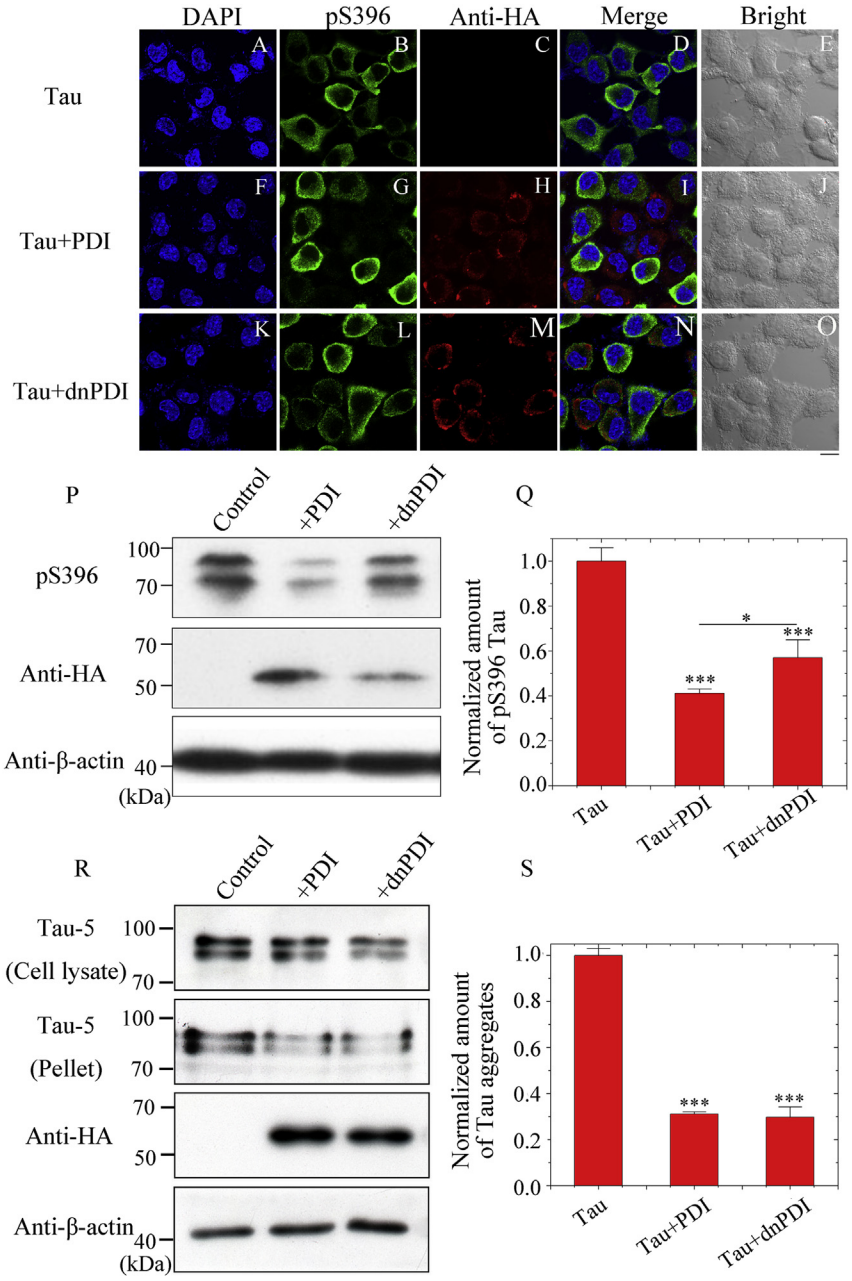

Fig. 2. Both wild-type PDI and its quadruple cysteine mutant significantly inhibit pathological phosphorylation and abnormal aggregation of Tau in cells. SH-SY5Y cells stably expressing full-length human Tau were cultured for 2 days. These cells were then transiently expressed HA-tagged wild-type PDI (F-J; or P and R, +PDI) or HA-tagged dnPDI (K−O; or P and R, +dnPDI) and incubated with 10 μM Congo red for 3 days, or directly incubated with 10 μM Congo red for 3 days (A-E; or P and R, control); fixed, permeabilized, immunostained with the anti-pS396 antibody (green) and anti-HA antibody (red), stained with DAPI (blue), and observed by confocal microscopy; or detected by Western blot. The scale bar represents 10 μm (A−O). We have replaced images A-O with better-quality images. (P) The cell lysates from the above cells were probed by the anti-pS396 antibody, anti-HA antibody, and anti-β-actin antibody, respectively. We have replaced the image of the HA blot with an image from the same blot probed for S396 Tau and β-actin. (Q) The normalized amount of pS396 Tau in SH-SY5Y cells expressing full-length Tau and PDI was determined as a ratio of the density of pS396 Tau bands over the density of β-actin band in cell lysates. The normalized amount of pS396 Tau is expressed as the mean ± S.D. (with error bars) of values obtained in 3 independent experiments. Tau + PDI, $p = 0.00077$; Tau + dnPDI, $p = 0.00085$. (R) The sarkosyl-insoluble pellets from the above cells were probed using Tau-5, and the corresponding cell lysates were probed using Tau-5, the anti-HA antibody, and anti-β-actin antibody, respectively. All blots also show the position of the molecular-weight markers (P and R). (S) The normalized amount of insoluble Tau aggregates in SH-SY5Y cells expressing full-length Tau and PDI was determined as a ratio of the density of insoluble Tau aggregate bands over

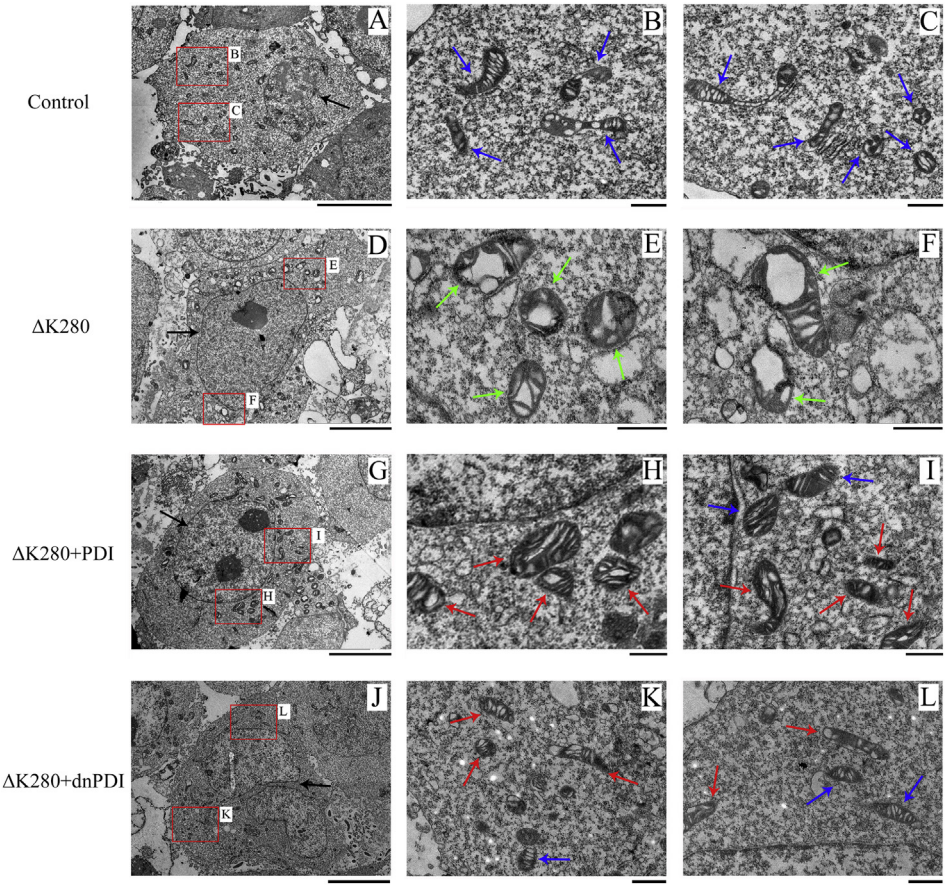

Fig. 3. TEM images show that both wild-type PDI and its quadruple cysteine mutant protect against mitochondrial damage in HEK-293T cells caused by aberrant aggregation of Tau and are induced by Tau oligomers. HEK-293T cells stably expressing ΔK280 of full-length human Tau were cultured for 2 days. These cells were then transiently expressed HA-tagged wild-type PDI (G–I) or HA-tagged dnPDI (J–L) and incubated with 5 μM Tau oligomers for 2 days, or directly incubated with 5 μM Tau oligomers for 2 days (D–F). HEK-293T cells transfected with an empty vector and incubated with HEPES buffer were used as a control (A–C). The enlarged regions B–C, E–F, H–I, and K-L, show twenty-five-fold enlarged images from A, D, G, and J, respectively, and display the detailed structures of mitochondria in HEK-293T cells. Nuclei are highlighted using black arrows (A, D, G, and J). The morphology of normal mitochondria in HEK-293T cells incubated with HEPES buffer (B and C) or in HEK-293T cells expressing ΔK280 of full-length Tau and wild-type PDI (I) or dnPDI (K and L) incubated with 5 μM Tau oligomers, which are highlighted by using blue arrows, was tubular or round. Tau oligomer treatment caused severe mitochondrial impairment in HEK-293T cells expressing ΔK280 (E and F). Most of the mitochondria in the cells (~70%) became swollen and vacuolized, which is highlighted by green arrows. In contrast, Tau oligomer treatment did not cause severe mitochondrial impairment in HEK-293T cells expressing ΔK280 and wild-type PDI (H and I) or dnPDI (K and L), and only a small number of mitochondria with swollen cristae or with disarranged cristae were observed in the cells (highlighted by red arrows). Samples were negatively stained using 2% uranyl acetate and lead citrate. The scale bars represent 5 μm for A, D, G, and J and 0.5 μm for B–C, E–F, H–I, and K–L.

SH-SY5Y cells expressing both Tau and PDI were significantly decreased by wild-type PDI and its quadruple cysteine mutant dnPDI (red fluorescence) (Fig. 2A–O and S3A–O). To gain a quantitative understanding of how PDI might modulate Tau phosphorylation in cells, we used Western blotting to probe cell lysates from the above cells for phosphorylated Tau, PDI, and β-actin using the

that of the total Tau bands in cell lysates. The normalized amounts of insoluble Tau aggregates are expressed as mean ± S.D. (with error bars) of values obtained in 3 independent experiments. Tau + PDI, $p = 0.00011$; Tau + dnPDI, $p = 0.000011$. Statistical analyses were performed using the Student *t*-test. Values of $p < 0.05$ indicate statistically significant differences. The following notation is used throughout: *, $p < 0.05$; **, $p < 0.01$; and ***, $p < 0.001$ relative to full-length Tau (a control, Q and S).

anti-pS396 antibody, anti-HA antibody, and anti-β-actin antibody, respectively (Fig. 2P and S3P). The normalized amount of pS396 Tau or pS396 ΔK280 in SH-SY5Y cells stably expressing full-length Tau or ΔK280 (Fig. 2Q and S3Q) and transiently expressing PDI was determined as a ratio of the density of pS396 Tau bands or pS396 ΔK280 bands over the density of β-actin band in the cell lysates. SH-SY5Y cells stably expressing full-length Tau (Fig. 2Q) or ΔK280 (Fig. S3Q) were used as a control. The densities of the pS396 Tau bands in the control cell lysates were much higher than those of the pS396 Tau bands in the cell lysates from cells transfected with wild-type PDI or dnPDI (Fig. 2P and S4A), and a significantly lower amount of full-length Tau was phosphorylated at Ser-396 in cells expressing PDI than did in control cells (0.411 ± 0.019 for Tau + PDI versus 1.000 ± 0.059 for Tau alone, $p = 0.00077$; 0.570 ± 0.080 for Tau + dnPDI versus 1.000 ± 0.059 for Tau alone, $p = 0.00085$) (Fig. 2Q). There was a significant difference between PDI and dnPDI ($p = 0.014$) (Fig. 2Q). We found that PDI exhibited a similar but weaker inhibitory effect on phosphorylation of ΔK280 than that on phosphorylation of full-length Tau (Fig. 2 and S3, P and Q). A significantly lower amount of ΔK280 was phosphorylated at Ser-396 in cells expressing PDI than did in control cells (0.708 ± 0.010 for ΔK280 + PDI versus 1.000 ± 0.006 for ΔK280 alone, $p = 0.00000093$; 0.717 ± 0.052 for ΔK280 + dnPDI versus 1.000 ± 0.006 for ΔK280 alone, $p = 0.0051$) (Fig. S3Q). Together, these results demonstrate that both wild-type PDI and its quadruple cysteine mutant only having chaperone activity, significantly inhibit pathological phosphorylation of Tau in cells, highlighting the chaperone property of PDI.

To gain a quantitative understanding of how PDI might modulate Tau aggregation in cells, and to compare the amount of insoluble Tau aggregates in PDI-expressing cells with those in control cells, we used Western blotting to probe the sarkosyl-insoluble pellets from the above cells for insoluble Tau aggregates using Tau-5, and the corresponding cell lysates for the total Tau, PDI, and β-actin using Tau-5, the anti-HA antibody, and anti-β-actin antibody, respectively (Fig. 2R and S3R). The normalized amount of insoluble Tau aggregates in SH-SY5Y cells stably expressing full-length Tau or ΔK280 (Fig. 2S and S3S) and transiently expressing PDI was determined as a ratio of the density of insoluble Tau aggregate bands after sample ultracentrifugation over that of the total Tau bands in cell lysates. SH-SY5Y cells stably expressing full-length Tau (Fig. 2S) or ΔK280 (Fig. S3S) were used as a control. The densities of the insoluble Tau aggregate bands in the control pellets were much higher than those of the insoluble Tau aggregate bands in the pellets from cells transfected with wild-type PDI or dnPDI (Fig. 3R), and a significantly lower amount of insoluble Tau aggregates was observed in cells expressing PDI than did in control cells (0.324 ± 0.012 for Tau + PDI versus 1.000 ± 0.010 for Tau alone, $p = 0.00011$; 0.305 ± 0.053 for Tau + dnPDI versus 1.000 ± 0.010 for Tau alone, $p = 0.000011$) (Fig. 3S). We found that PDI exhibited a similar but weaker inhibitory effect on ΔK280 aggregation than that on full-length Tau aggregation (Fig. 2 and S3, R and S). A significantly lower amount of insoluble ΔK280 aggregates was observed in cells expressing PDI than did in control cells (0.499 ± 0.072 for ΔK280 + PDI versus 1.000 ± 0.008 for ΔK280 alone, $p = 0.0047$; 0.318 ± 0.018 for ΔK280 + dnPDI versus 1.000 ± 0.008 for ΔK280 alone, $p = 0.00000015$) (Fig. S3S). Therefore, abnormal aggregation of Tau was significantly inhibited by both wild-type PDI and its quadruple cysteine mutant only having chaperone activity. Together, these results demonstrate that PDI significantly inhibits Tau phosphorylation and aggregation in cells by acting as a chaperone.

PDI protects against mitochondrial damage in cells caused by Tau aggregation and induced by Tau oligomers

To address the questions of the relationship between Tau aggregation and mitochondrial damage, we used transmission electron microscopy (TEM) [67,68] to study the influences of expressed Tau on mitochondrial damage and expressed PDI on mitochondrial dynamics in HEK-293T cells incubated with 5 μM wild-type full-length Tau oligomers (Fig. 3). HEK-293T cells stably expressing ΔK280 of full-length Tau were cultured for 2 days, then transiently expressed HA-tagged wild-type PDI (Fig. 3G–I) or HA-tagged dnPDI (Fig. 3J–L) and incubated with 5 μM Tau oligomers for 2 days. HEK-293T cells stably expressing ΔK280 and directly incubated with 5 μM Tau oligomers for 2 days were used as a negative control (Fig. 3D–F). HEK-293T cells transfected with an empty vector and incubated with HEPES buffer were used as a positive control (Fig. 3A–C). The morphology of normal mitochondria in cells incubated with HEPES buffer (Fig. 3B and C) or in cells stably expressing ΔK280 and transiently expressing wild-type PDI (Fig. 3I) or dnPDI (Fig. 3K and L) incubated with 5 μM Tau oligomers, highlighted by blue arrows, was tubular or round. Tau oligomer treatment caused severe mitochondrial impairment in cells expressing ΔK280, most of the mitochondria in the cells (~70%) became swollen and vacuolized, and the mitochondrial cristae were broken, which is highlighted by green arrows (Fig. 3E and F). In contrast, Tau oligomer treatment did not cause severe mitochondrial impairment in cells stably expressing ΔK280 and transiently expressing wild-type PDI (Fig. 3H and I) or dnPDI (Fig. 3K and L), and only

a small number of mitochondria with swollen cristae or with disarranged cristae were observed in the cells (highlighted by red arrows) (Fig. 3H–I and K-L). Quantification of TEM images performed on three biological replicates show that both wild-type PDI and dnPDI protect against mitochondrial damage in cells caused by aberrant aggregation of Tau and are induced by Tau oligomers (Fig. S5). A significantly lower number of normal mitochondria was observed in cells expressing ΔK280 than did in control cells (0.334 ± 0.044 for ΔK280 versus 0.854 ± 0.014 for the control, $p = 0.000021$) (Fig. S5). By contrast, a significantly higher number of normal mitochondria was observed in cells expressing both ΔK280 and PDI than did in the control cells expressing ΔK280 alone (0.636 ± 0.014 for ΔK280 + PDI versus 0.334 ± 0.044 for ΔK280 alone, $p = 0.00018$; 0.640 ± 0.056 for ΔK280 + dnPDI versus 0.334 ± 0.044 for ΔK280 alone, $p = 0.00025$) (Fig. S5). Collectively, these data demonstrate that Tau oligomers cause much more severe mitochondrial impairment in the negative control cells than in cells expressing wild-type PDI or dnPDI. Therefore, PDI acts as a chaperone and protects against mitochondrial damage in cells caused by Tau aggregation and induced by Tau oligomers.

PDI significantly decreases Tau cytotoxicity resulting from Tau aberrant aggregation

To examine the role of Tau aggregation in cytotoxicity, we used flow cytometry with annexin V-fluorescein isothiocyanate (FITC) and propidium iodide (PI) staining [59,60,69–71] to study the influences of expressed Tau and PDI on toxicity in living cells incubated with 5 μM Tau oligomers (Fig. 4). SH-SY5Y (Fig. 4A–C) and HEK-293T (Fig. 4D–F) cells stably expressing ΔK280 of full-length Tau were cultured for 2 days, then transiently expressed HA-tagged wild-type PDI (Fig. 4B and E)

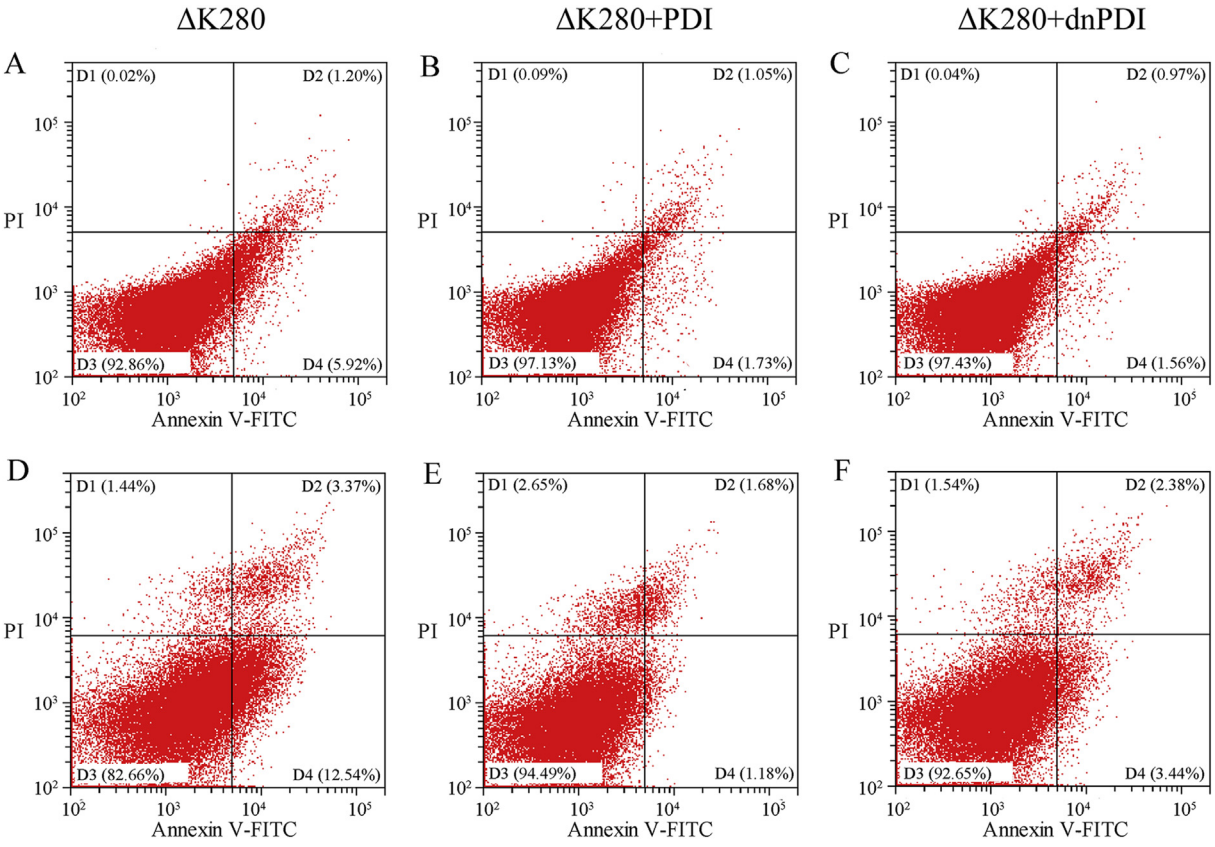

Fig. 4. Both wild-type PDI and its quadruple cysteine mutant significantly decrease Tau cytotoxicity resulting from Tau aberrant aggregation. SH-SY5Y (A–C) and HEK-293T (D–F) cells stably expressing ΔK280 of full-length human Tau were cultured for 2 days. These cells were then transiently expressed HA-tagged wild-type PDI (B and E) or HA-tagged dnPDI (C and F) and incubated with 5 μM Tau oligomers for 2 days, or directly incubated with 5 μM Tau oligomers for 2 days (A and D). SH-SY5Y (A) and HEK-293T (D) cells stably expressing ΔK280 of full-length Tau directly incubated with Tau oligomers were used as controls. The percentage of apoptotic cells was determined by flow cytometry. The four quadrants distinguished by annexin V-FITC/PI staining represent viable cells (D3 quadrant), early apoptotic cells (D4 quadrant), late apoptotic cells (D2 quadrant) and operation-damaged cells (D1 quadrant).

or HA-tagged dnPDI (Fig. 4C and F) and incubated with 5 μM Tau oligomers for 2 days. SH-SY5Y and HEK-293T cells stably expressing ΔK280 and directly incubated with 5 μM Tau oligomers for 2 days were used as negative controls (Fig. 4A and D). The percentage of early apoptotic cells among negative control living cells treated with 5 μM Tau oligomers for 2 days was 5.92% (Fig. 4A), which was significantly higher than that in SH-SY5Y cells treated with 5 μM Tau oligomers and expressing both ΔK280 and wild-type PDI (Fig. 4B, 1.73%) or dnPDI (Fig. 4C, 1.56%). We suspected that PDI blocked the intrinsic ability of Tau oligomers to induce apoptosis in cells. To test this hypothesis, we used one different cell type. The percentage of early apoptotic cells among negative control living cells treated with 5 μM Tau oligomers for 2 days was 12.54% (Fig. 4D), which was also significantly higher than that in HEK-293T cells treated with 5 μM Tau oligomers and expressing both ΔK280 and wild-type PDI (Fig. 4E, 1.18%) or dnPDI (Fig. 4F, 3.44%). Interestingly, when treated with Tau oligomers, ΔK280-expressing cells, cells expressing both ΔK280 and wild-type PDI, and cells expressing both ΔK280 and dnPDI all showed similar rates of late apoptosis (Fig. 4A–C for SH-SY5Y cells, 1.20%, 1.05%, and 0.97% respectively; Fig. 4D–F for HEK-293T cells, 3.37%, 1.68%, and 2.38% respectively).

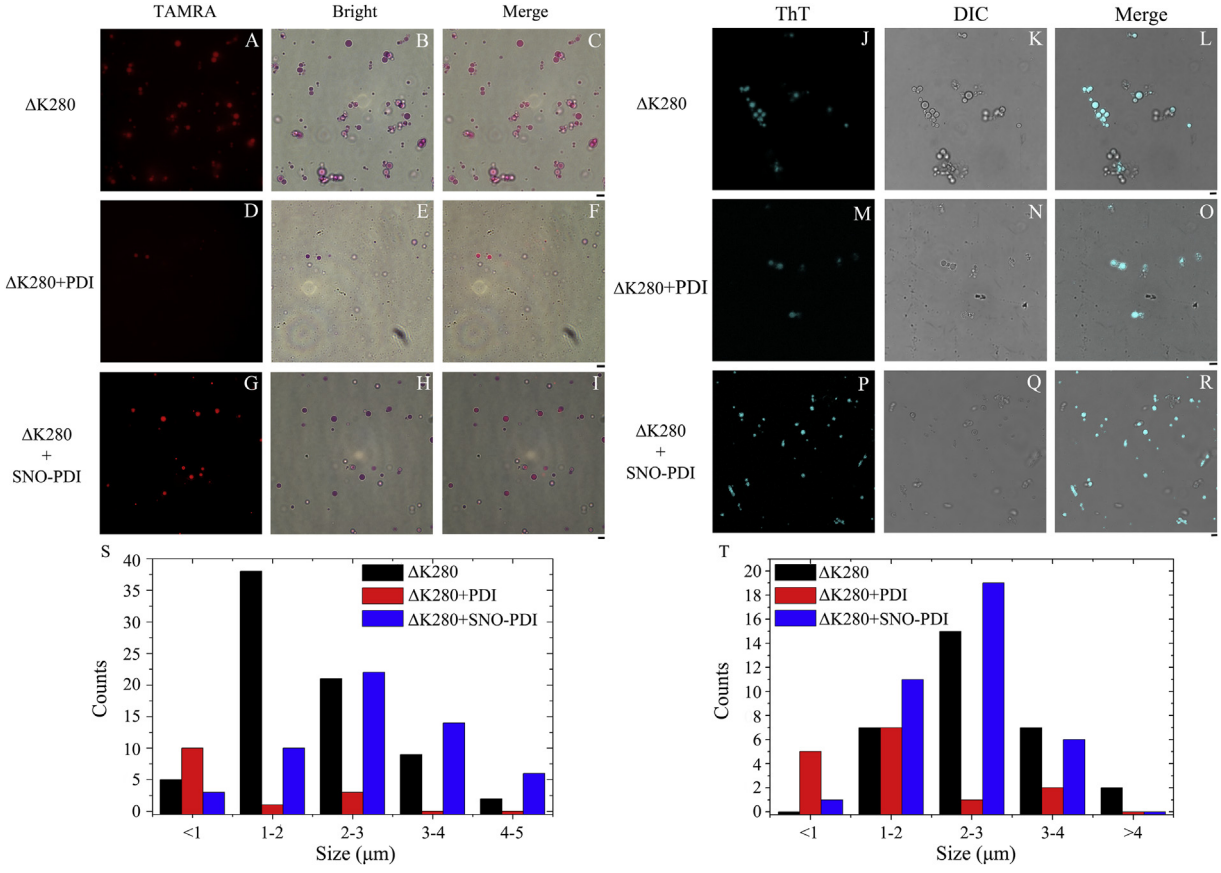

Fig. 5. Liquid-liquid phase separation of Tau is modulated by PDI and S-nitrosylation of this molecular chaperone. (A–R) 100 μM ΔK280 of human Tau fragment $Tau_{244-372}$ was incubated with 10 mM HEPES buffer (pH 7.4) containing 100 mM NaCl, 25 μM heparin and 12.5% Ficoll 70 (A–C and J–L) or incubated with the same buffer further containing 100 μM wild-type PDI (D–F and M–O) or 100 μM SNO-PDI (G–I and P–R) on ice to induce liquid-liquid phase separation for 30 min. (A–I) ΔK280 was labeled by TAMRA (red fluorescence), and liquid droplets of 100 μM ΔK280 in HEPES (Bright: purple; Merge: red) were observed by confocal microscopy, with excitation at 546 nm. (J–R) ΔK280 in liquids was stained with 100 μM ThT (cyan fluorescence), and liquid droplets of ΔK280 (Merge: cyan) were observed by DIC confocal microscopy, with excitation at 440 nm. The scale bars represent 4 μm. Histograms showing the distribution of the counts of different-size liquid droplets of 100 μM ΔK280 labeled with TAMRA (S) or stained by ThT (T) in HEPES (black)/100 μM wild-type PDI (red)/100 μM SNO-PDI (blue). All protein phase separation experiments were repeated three times, and the results were reproducible.

Collectively, these data demonstrate that Tau oligomers cause much more severe early apoptosis in the negative control cells than in cells expressing wild-type PDI or dnPDI. Therefore, PDI acts as a chaperone and significantly decreases cytotoxicity caused by Tau aggregation and induced by Tau oligomers.

Liquid-liquid phase separation of Tau is modulated by PDI and S-nitrosylation of this molecular chaperone

Crowding agents can be used to mimic the cellular crowding environment where liquid-liquid phase separation of Tau occurs [24]. For mimicking the

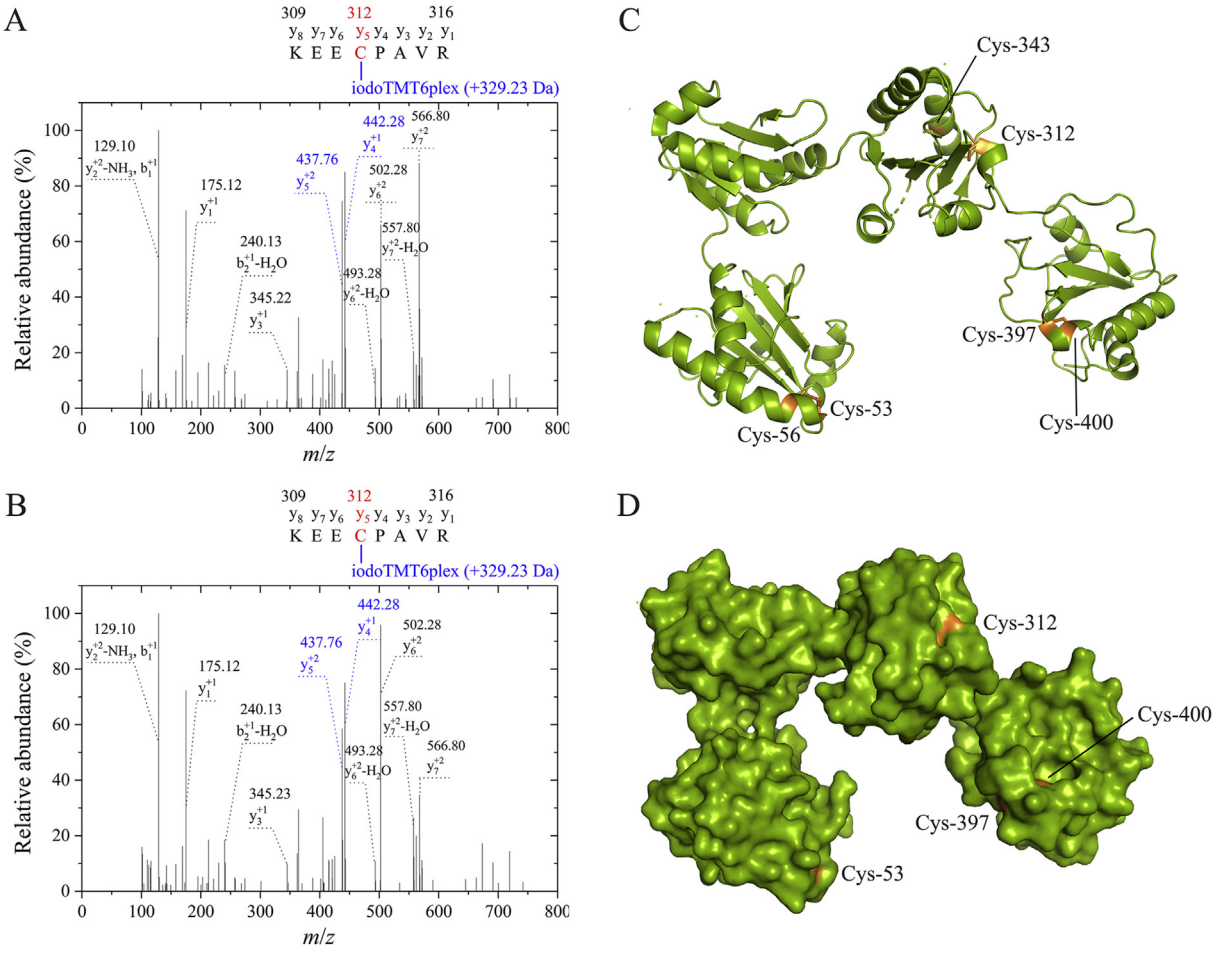

Fig. 6. Characterization of S-nitrosylated PDI by mass spectrometry. To produce SNO-PDI, purified wild-type PDI (50 μg) was treated with S-nitrosocysteine at a molar ratio of 1:100 (A) or 500 μM S-nitrosoglutathione (B) for 1 h at 25 °C to allow S-nitrosylation to occur. 20 mM S-methyl methanethiosulfonate (MMTS) was added to block free cysteine thiols, and excess MMTS was removed by ice-cold acetone precipitation followed by centrifugation at 2000 *g* for 10 min. SNO modification sites of PDI were reduced by 20 mM ascorbate and labeled with iodoTMT-127 according to the iodoTMT™ labeling kit (Thermo Scientific). 20 mM DTT was added to quench the reaction, and the sample was treated with iodoacetamide. The sample was then digested by trypsin (0.4 mg trypsin per 1 mg of protein) at 37 °C overnight and acidified by the addition of trifluoroacetic acid after digestion. We cleaned up peptides using 50 mg C18 SPE columns, and frozen and lyophilized peptides using a vacuum concentrator. IodoTMT reagent-labeled peptides were enriched with anti-TMT resin and then analyzed with nano-LC-MS/MS. An MS^2 analysis of IodoTMT6plex-labeled parent peptide $K^{309}EECPAVR^{316}$ digested by trypsin (A and B). Analysis of the y-ions indicates irreversible labeling of SNO-Cys with IodoTMT6plex (+329.23 Da) (A and B), demonstrating S-nitrosylation of Cys-312 in wild-type PDI. Ribbon (C) and surface (D) representations of the structure of oxidized wild-type human PDI (green) (residues 18–479) containing two catalytic domains a (the left bottom) and a' (the right bottom), domain b (the left top), and a large hydrophobic pocket embedded in domain b' (the right top) (PDB entry 4EL1) [46]. Human PDI has six cysteine residues (orange), two of which (Cys-312 and Cys-343) are present as free cysteines (C). Two disulfide bonds (orange) are formed between Cys-53 and Cys-56, and between Cys-397 and Cys-400. (C and D) Cys-312 is a reactive Cys residue half exposed on the surface, whereas Cys-343 is deeply buried inside this enzyme.

Tau phase separation *in vivo*, polyanionic cofactors, such as heparin, have been used to induce the Tau phase separation *in vitro* [24]. In this article, we used confocal microscopy to study the influences of crowding environment, and heparin on the formation of Tau phase-separated droplets. 100 μM ΔK280 of $Tau_{244-372}$, the microtubule binding region of Tau, labeled by 5(6)-carboxy-tetramethylrhodamine N-succinimidyl ester (TAMRA, red fluorescence), was incubated with 10 mM HEPES buffer (pH 7.4) containing 100 mM NaCl, 25 μM heparin, and 12.5% Ficoll 70 on ice to induce liquid-liquid phase separation for 30 min. ΔK280 formed liquid droplets (Bright: purple; Merge: red) in HEPES buffer containing both a crowding agent and heparin (Figs. 5A–C, S6A, S6D, and S7A–C). Because Ficoll 70 is a copolymer of two short building blocks sucrose and epichlorohydrin [72], sucrose was used as a control for this crowding agent. 100 μM ΔK280 was incubated with 10 mM HEPES buffer (pH 7.4) containing 100 mM NaCl, 25 μM heparin, and 12.5% sucrose or incubated with HEPES containing 100 mM NaCl, 12.5% Ficoll 70, and no heparin, on ice for 30 min as controls. ΔK280 did not form liquid droplets in HEPES buffer in the absence of a crowding agent or heparin (Fig. S6B, C, E, and F). We conclude that crowding environment and heparin are important for liquid-liquid phase separation of Tau.

In neurodegenerative diseases, pathological fibrils could arise from liquid droplets [16,24,73]. To understand why PDI suppresses Tau aggregation and toxicity in cells (this work) and how aberrantly S-nitrosylated PDI contributes to the pathogenesis of AD and related neurodegenerative diseases [48,50–53,74,75], we first tested the hypothesis that liquid-liquid phase separation of Tau, which initiates Tau aggregation [24,26], might be modulated by PDI and S-nitrosylation of this chaperone. 100 μM ΔK280 of $Tau_{244-372}$ was incubated with 10 mM HEPES buffer (pH 7.4) containing 100 mM NaCl, 25 μM heparin, and 12.5% Ficoll 70 (Figs. 5 and S7, A–C and J–L) or incubated with the same buffer further containing 100 μM oxidized wild-type PDI (Figs. 5 and S7, D–F and M–O) or 100 μM S-nitrosylated PDI (SNO-PDI) (Figs. 5 and S7, G–I and P–R) on ice to induce liquid-liquid phase separation for 30 min. SNO-PDI was produced by the reaction of oxidized wild-type PDI with the physiological NO donor S-nitrosocysteine [50] and characterized by nano-LC-MS/MS. Analysis of the y-ions in Fig. 6A and B indicated irreversible labeling of SNO-Cys-312 of oxidized wild-type PDI with IodoTMT6plex (+329.23 Da). Cartoon and surface structures of oxidized wild-type PDI (PDB entry 4EL1) [46] show this enzyme has six cysteine residues, two of which (Cys-312 and Cys-343) are present as free cysteines and located in domain b' (Fig. 6C and D). Two disulfide bonds (orange) are formed between Cys-53 and Cys-56 in the catalytic domain a, and between Cys-397 and Cys-400 in the catalytic domain a' (Fig. 6C). Cys-312, the most solvent-exposed Cys in PDI, is a reactive Cys residue half exposed on the surface, whereas Cys-343 is deeply buried inside this enzyme (Fig. 6C and D). Together, these results demonstrate that Cys-312 of PDI is S-nitrosylated when treated with S-nitrosocysteine or S-nitrosoglutathione (Fig. 6). No other damage was observed during S-nitrosylation of PDI (Fig. 6). Thus, our results would be compatible with the idea that the protein *in vivo* is modified in low abundance. ΔK280 was labeled with TAMRA (red), and liquid droplets of ΔK280 in HEPES (Bright: purple; Merge: red) were observed by confocal microscopy with excitation at 546 nm (Figs. 5 and S7, A–I). ΔK280 in liquids was also stained with thioflavin T (ThT, cyan), a fluorescent dye that specifically binds to β-sheet structures of liquids [24,26,31] or fibrils [2,59,60,69], and liquid droplets of ΔK280 (Merge: cyan) were observed by differential interference contrast (DIC) confocal microscopy with excitation at 440 nm (Figs. 5 and S7, J–R). ΔK280 formed abundant liquid droplets with diameters of 2–4 μm and β-sheet-rich structures in HEPES buffer containing Ficoll 70, heparin, and no PDI (Figs. 5 and S7, A–C and J–L). However, ΔK280 produced only a small number of liquid droplets with less β-sheet structures and smaller sizes (~1 μm) in HEPES buffer containing Ficoll 70, heparin, and wild-type PDI (Figs. 5 and S7, D–F and M–O). Either the number or the ThT fluorescence intensity of ΔK280 phase-separated droplets in the presence of wild-type PDI was much less than that in the absence of PDI (Figs. 5 and S7, A–F and J–O). Interestingly, ΔK280 also formed abundant liquid droplets with sizes of 2–4 μm and cross-β rich structures in HEPES buffer containing Ficoll 70, heparin, and SNO-PDI (Figs. 5 and S7, G–I and P–R). Quantification of images of liquid droplets of ΔK280 labeled with TAMRA or stained by ThT shows that SNO-PDI protects against a sharp decrease in the counts of liquid droplets with sizes ranging from 1 to 2 μm to >4 μm caused by wild-type PDI (Figs. 5 and S7, S and T). Together, these results demonstrate that PDI, which directly interacts with Tau in cells, acts as a Tau chaperone and suppresses the formation of Tau phase-separated droplets, but S-nitrosylation of PDI antagonizes this inhibitory effect. Therefore, liquid-liquid phase separation of Tau is modulated by PDI and S-nitrosylation of this molecular chaperone.

Liquid droplets of Tau selectively recruit wild-type PDI, but S-nitrosylation of this molecular chaperone abrogates the recruitment

To understand how liquid-liquid phase separation of Tau is modulated by PDI and its S-nitrosylation,

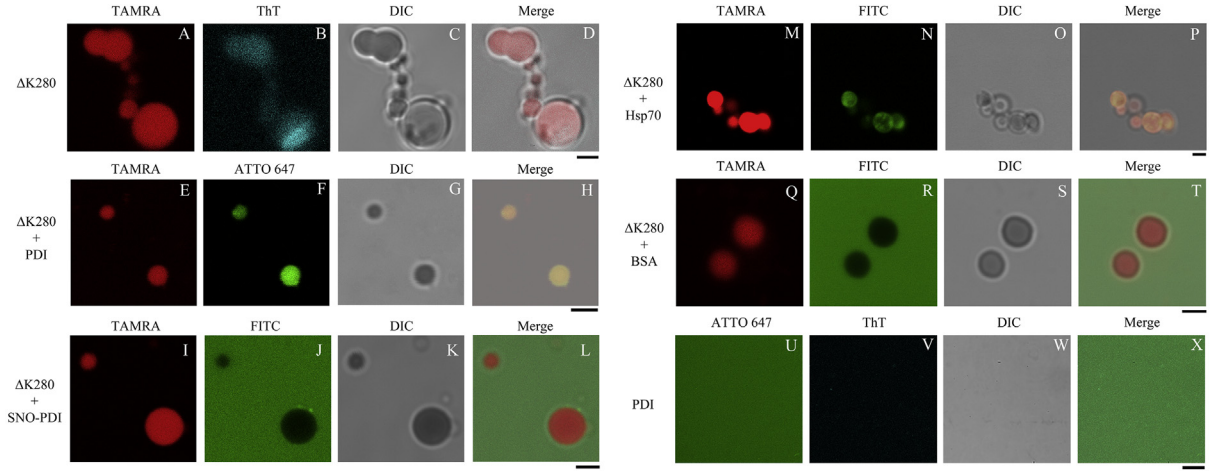

Fig. 7. Liquid droplets of Tau selectively recruit wild-type PDI, but S-nitrosylation of this molecular chaperone abrogates the recruitment. (A–T) 100 μM ΔK280 of $Tau_{244-372}$ was incubated with 10 mM HEPES buffer (pH 7.4) containing 100 mM NaCl, 25 μM heparin and 12.5% Ficoll 70 (A–D) or incubated with the same buffer further containing 100 μM wild-type PDI (E–H) or 100 μM SNO-PDI (I–L) or 100 μM Hsp70 (M–P) or 100 μM BSA (Q–T) on ice to induce liquid-liquid phase separation for 30 min. ΔK280 was labeled by TAMRA (red fluorescence). (A–D) ΔK280 in liquids was stained with 100 μM ThT (cyan fluorescence), and liquid droplets of ΔK280 (red; Merge: pink) were observed by DIC confocal microscopy, with excitation at 546 nm and 440 nm, respectively. (E–H) Wild-type PDI was labeled by ATTO 647 (green fluorescence), and liquid droplets of ΔK280 (red; Merge: light yellow) were observed by DIC confocal microscopy, with excitation at 546 nm and 647 nm, respectively. (I–L) SNO-PDI was labeled by FITC (green fluorescence), and liquid droplets of ΔK280 (red; Merge: dark pink) were observed by DIC confocal microscopy, with excitation at 546 nm and 488 nm, respectively. (M–P) Hsp70, a typical molecular chaperone, and positive control, were also labeled by FITC, and liquid droplets of ΔK280 (Merge: light yellow tinged orange) were observed by DIC confocal microscopy. (Q–T) BSA, a negative control, was also labeled by FITC, and liquid droplets of ΔK280 (Merge: dark red) were observed by DIC confocal microscopy. (U–X) Wild-type PDI was labeled by ATTO 647, and neither phase separation nor ThT staining for 100 μM wild-type PDI in HEPES was observed by DIC confocal microscopy, with excitation at 647 nm and 440 nm, respectively. 100 μM wild-type PDI was incubated with 10 mM HEPES buffer (pH 7.4) containing 100 mM NaCl, 25 μM heparin, and 12.5% Ficoll 70 on ice for 30 min as controls. The scale bars represent 2 μm. All protein phase separation experiments were repeated three times, and the results were reproducible.

we next tested the hypothesis that liquid droplets of Tau might selectively recruit PDI and S-nitrosylation of this chaperone might modulate the recruitment. 100 μM ΔK280 of $Tau_{244-372}$ was incubated with 10 mM HEPES buffer (pH 7.4) containing 100 mM NaCl, 25 μM heparin, and 12.5% Ficoll 70 (Figs. 7, S8, and S9, A–D) or incubated with the same buffer further containing 100 μM wild-type PDI (Figs. 7, S8, and S9, E–H) or 100 μM SNO-PDI (Figs. 7, S8, and S9, I–L) or 100 μM Hsp70 (Figs. 7, S8, and S9, M–P) or 100 μM bovine serum albumin (BSA) (Figs. 7, S8, and S9, Q–T) on ice to induce liquid-liquid phase separation for 30 min. ΔK280 was labeled by TAMRA (red), ΔK280 in liquids was stained with ThT (cyan), and liquid droplets of ΔK280 (red; Merge: pink) were observed DIC confocal microscopy with excitation at 546 nm and 440 nm, respectively (Figs. 7, S8, and S9, A–D). Once again, ΔK280 formed liquid droplets with diameters of 2–4 μm and β-sheet-rich structures in HEPES buffer containing Ficoll 70, heparin, and no PDI (Figs. 7, S8, and S9, A–D). ΔK280 and wild-type PDI were labeled with TAMRA and ATTO 647 (green fluorescence), respectively, and liquid droplets of ΔK280 (red; Merge: light yellow) were observed DIC confocal microscopy with excitation at 546 nm and 647 nm, respectively (Figs. 7, S8, and S9, E–H). ΔK280 and SNO-PDI were labeled with TAMRA and FITC (green fluorescence), respectively, and liquid droplets of ΔK280 (red; Merge: dark pink) were observed DIC confocal microscopy with excitation at 546 nm and 488 nm, respectively (Figs. 7, S8, and S9, I–L). DIC and fluorescence images show that wild-type PDI was recruited and concentrated into liquid droplets of ΔK280 with smaller sizes (~1 μm) (Figs. 7, S8, and S9, E–H). However, SNO-PDI was excluded from liquid droplets of ΔK280 with diameters of 2–4 μm. Instead, SNO-PDI was evenly distributed in the dilute phase (Figs. 7, S8, and S9, I–L). Hsp70, a typical chaperone, was used as a positive control. ΔK280 and Hsp70 were labeled with TAMRA and FITC (green), respectively, and liquid droplets of ΔK280 (red; Merge: light yellow tinged orange) were observed DIC confocal microscopy with excitation at 546 nm and 488 nm, respectively (Figs. 7, S8, and S9, M–P). Similar to wild-type PDI,

Hsp70 was also recruited and concentrated into liquid droplets of ΔK280 with smaller sizes (Figs. 7, S8, and S9, M–P). BSA was used as a negative control. ΔK280 and BSA were labeled with TAMRA and FITC (green), respectively, and liquid droplets of ΔK280 (red; Merge: dark red) were observed DIC confocal microscopy with excitation at 546 nm and 488 nm, respectively (Figs. 7, S8, and S9, Q–T). Similar to SNO-PDI, BSA was also excluded from liquid droplets of ΔK280 with diameters of 2–4 μm. Instead, BSA was evenly distributed in the dilute phase (Figs. 7, S8, and S9, Q–T). Therefore, the specific interaction between Tau and wild-type PDI was once again observed. Furthermore, control experiments showed that wild-type PDI did not form liquid droplets in HEPES buffer containing Ficoll 70 and heparin and could not be stained by ThT (Figs. 7, S8, and S9, U–X). Wild-type PDI was labeled with ATTO 647 (green fluorescence) and stained with ThT (cyan), neither phase separation

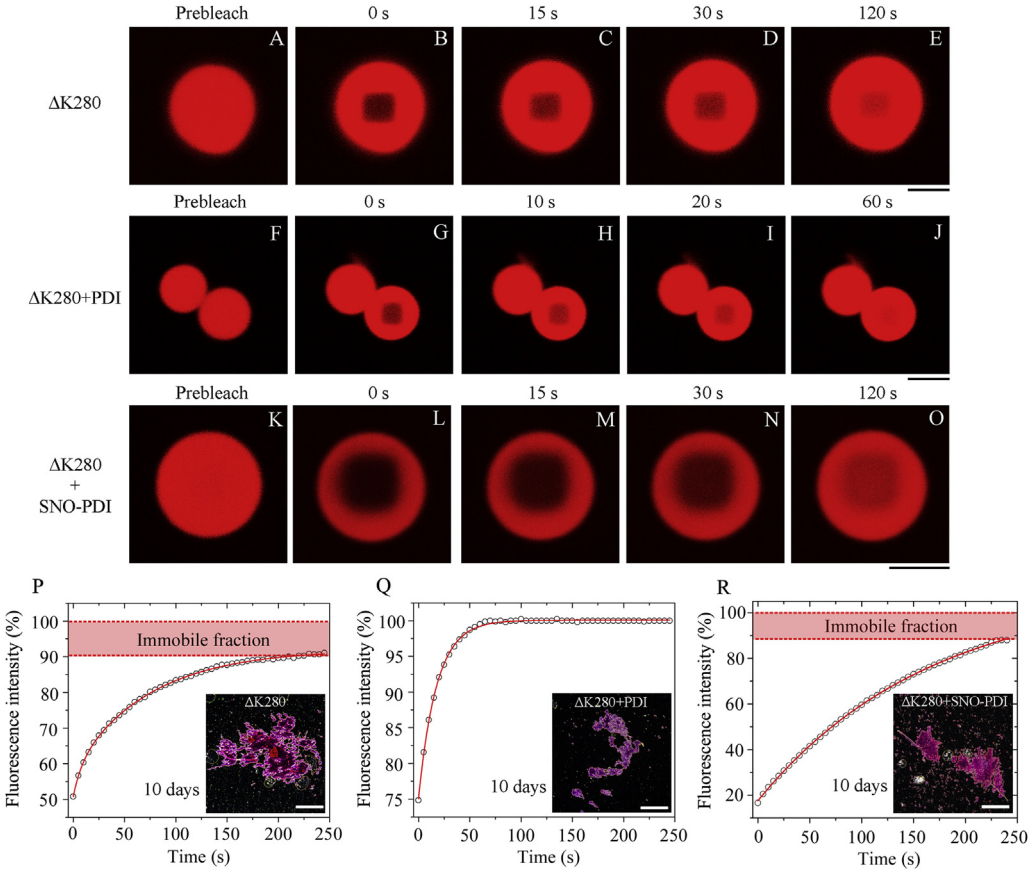

Fig. 8. Dynamics of Tau phase-separated droplets is modulated by PDI and S-nitrosylation of this molecular chaperone. (A–O) Time course of FRAP after internal photobleaching of liquid droplets of 100 μM ΔK280 of $Tau_{244-372}$ incubated with 10 mM HEPES buffer (pH 7.4) containing 100 mM NaCl, 25 μM heparin and 12.5% Ficoll 70 (A-E and P) or incubated with the same buffer further containing 100 μM wild-type PDI (F-J and Q) or 100 μM SNO-PDI (K–O and R). The internal photobleaching is marked by a black square. Prebleaching represents the time before photobleaching (A, F, and K) and time 0 indicates that for photobleaching (B, G, and L). The fluorescence recovery time is indicated on top of the corresponding recovery image (C–E, H–J, and M–O). ΔK280 was incubated with HEPES on ice to induce liquid-liquid phase separation for 30 min and hydrogel formation for 10 days. ΔK280 was labeled by TAMRA (red fluorescence), and both liquid droplets (red, A–O) and hydrogels (purple, P–R, the inset) of ΔK280 were observed by confocal microscopy. The scale bars represent 2 μm for A–O and 500 μm for P–R, the inset. (P–R) Fluorescence intensity changes in a bleached region over time (open circle) were normalized against the first time point before photobleaching. The solid red lines show the best single exponential fit for the fluorescence intensity-time curves. FRAP of liquid droplets of ΔK280 incubated with HEPES (P) or incubated with wild-type PDI (Q) or SNO-PDI (R) revealed a fluorescence recovery rate of $(1.64 \pm 0.05) \times 10^{-2}\ s^{-1}$ or $(5.67 \pm 0.05) \times 10^{-2}\ s^{-1}$ or $(6.04 \pm 0.06) \times 10^{-3}\ s^{-1}$ with an immobile Tau molecule fraction of 10% or 0% or 12%. The inset in P–Q shows that wild-type PDI remarkably reduced the number of hydrogels of ΔK280, but S-nitrosylation of PDI abrogates the inhibition. All FRAP experiments were repeated three times, and the results were reproducible.

nor ThT staining for 100 μM wild-type PDI in HEPES was observed by DIC confocal microscopy with excitation at 647 nm and 440 nm, respectively. Instead, wild-type PDI was evenly distributed in the dilute phase (Figs. 7, S8, and S9, U–X). Together, these results demonstrate that liquid droplets of Tau selectively recruit wild-type PDI, but S-nitrosylation of this molecular chaperone abrogates the recruitment.

Dynamics of Tau phase-separated droplets is modulated by PDI and S-nitrosylation of this molecular chaperone

We have shown that wild-type PDI is selectively recruited by liquid droplets of Tau and significantly inhibits Tau phase separation, but S-nitrosylation of PDI antagonizes the recruitment and inhibition. Recently, fluorescence recovery after photobleaching (FRAP) of a fraction of Tau droplets has been used to evaluate the mobility and dynamics of Tau molecules in the droplets [24,25,30,32,34]. We then analyzed the dynamics of Tau molecules within the liquid droplets of 100 μM ΔK280 of $Tau_{244-372}$ incubated with 10 mM HEPES buffer (pH 7.4) containing 100 mM NaCl, 25 μM heparin, and 12.5% Ficoll 70 (Figs. 8 and S10, A–E and P) or incubated with the same buffer further containing 100 μM wild-type PDI (Figs. 8 and S10, F–J and Q) or 100 μM SNO-PDI (Figs. 8 and S10, K–O and R) by FRAP measurements. ΔK280 was incubated with HEPES on ice to induce liquid-liquid phase separation for 30 min and hydrogel formation for 10 days (Figs. 8 and S10). ΔK280 was labeled with TAMRA (red), and both liquid droplets (red, Figs. 8 and S10, A–O) and hydrogels (purple, Fig. 8P–R, the inset) of ΔK280 were observed by confocal microscopy. Fluorescence intensity changes in a bleached region over time (open circle) were plotted, and the solid red lines show the best single exponential fit for the fluorescence intensity-time curves (Figs. 8 and S10, P–R). After photobleaching of ΔK280 droplets formed in HEPES buffer containing Ficoll 70, heparin, and no PDI, a two-third recovery of the Tau fluorescence was observed when the fluorescence recovery time was 120 s, and a relatively slow recovery rate of $(1.64 \pm 0.05) \times 10^{-2}$ s^{-1} or $(5.37 \pm 0.62) \times 10^{-3}$ s^{-1} with about 10% of immobile Tau molecule fraction in the droplets was also observed (Figs. 8 and S10, A–E and P). After photobleaching of ΔK280 droplets formed in HEPES buffer containing Ficoll 70, heparin, and wild-type PDI, however, a complete recovery of the Tau fluorescence was observed when the fluorescence recovery time was 60 s, and a recovery rate of $(5.67 \pm 0.05) \times 10^{-2}$ s^{-1} or $(3.41 \pm 0.06) \times 10^{-2}$ s^{-1} that was about 5-fold faster than that in the absence of PDI, with an ~0% immobile Tau molecule fraction in the droplets, was also observed (Figs. 8 and S10, F–J and Q). Interestingly, after photobleaching of ΔK280 droplets formed in HEPES buffer containing Ficoll 70, heparin, and SNO-PDI, a half-recovery of the Tau fluorescence was observed when the fluorescence recovery time was 120 s, and a recovery rate of $(6.04 \pm 0.06) \times 10^{-3}$ s^{-1} or $(3.38 \pm 0.05) \times 10^{-3}$ s^{-1} that was similar to that in the absence of PDI, with an ~12% immobile Tau molecule fraction in the droplets, was also observed (Figs. 8 and S10, K–O and R). The inset in Fig. 8P–R shows that wild-type PDI remarkably reduced the number of hydrogels of ΔK280, but SNO-PDI did not reduce the number of hydrogels of ΔK280. Together, these results demonstrate that PDI remarkably accelerates FRAP of liquid droplets of Tau and significantly inhibits the phase transition of Tau from liquid droplets to hydrogels, but S-nitrosylation of PDI abrogates the acceleration and inhibition. Therefore, the dynamics of Tau phase-separated droplets is modulated by PDI and S-nitrosylation of this molecular chaperone.

Wild-type PDI significantly inhibits stress granule formation of Tau in cells

We have shown that wild-type PDI, which directly interacts with Tau in cells, acts as a Tau chaperone, and suppresses the formation of Tau phase-separated droplets. We next tested the hypothesis that wild-type PDI might suppress stress granule formation of Tau in cells. HEK-293T cells transiently expressing full-length Tau labeled by EGFP (green) with endogenous TIA-1, cultured for 1 day, then incubated with 0 (Fig. 9A–E) or 500 μM sodium arsenite for 45 min (Fig. 9F–J), were immunostained with the anti-TIA-1 antibody (magenta), stained with DAPI (blue), and observed by confocal microscopy. HEK-293T cells transiently expressing both full-length Tau labeled by EGFP and HA-tagged wild-type PDI with endogenous TIA-1, cultured for 1 day, then incubated with 0 (Fig. 9K–O) or 500 μM $NaAsO_2$ for 45 min (Fig. 9P–T), were also immunostained with the anti-HA antibody (red) and anti-TIA-1 antibody (magenta), stained with DAPI (blue), and observed by confocal microscopy. Magenta dots indicated TIA-1-positive stress granules formed in HEK-293T cells under stress conditions (Fig. 9H and R). In unstressed conditions, TIA-1 was evenly distributed in cells (Fig. 9C and M). We used white arrows to highlight TIA-1-positive stress granules containing Tau in HEK-293T cells in stress conditions and found that wild-type PDI remarkably reduces the number of stress granules per cell (Fig. 9G, H, J, Q, R, and T). Quantification of images of TIA-1-positive stress granules performed on 3 biological replicates show that wild-type PDI significantly inhibits stress granule formation of Tau in cells (Fig. S11).

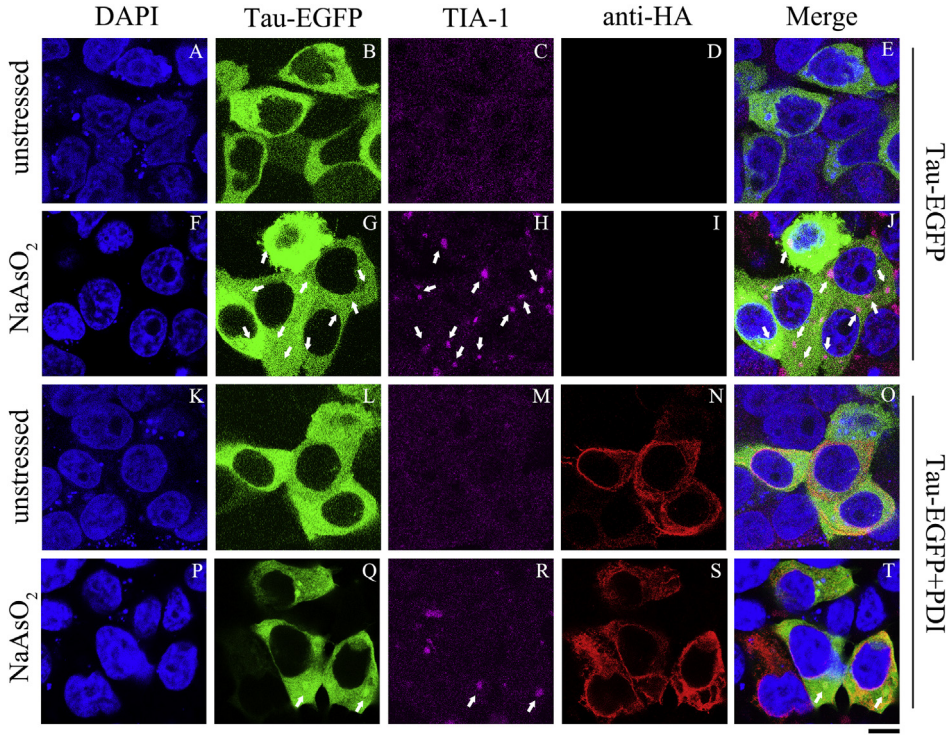

Fig. 9. Wild-type PDI significantly inhibits stress granule formation of Tau in cells. HEK-293T cells transiently expressing full-length human Tau labeled by EGFP (green) with endogenous TIA-1 were cultured for 1 day, then incubated with 0 (A-E, unstressed) or 500 μM sodium arsenite for 45 min (F–J), fixed, permeabilized, immunostained with the anti-TIA-1 antibody (magenta), stained with DAPI (blue), and observed by confocal microscopy. HEK-293T cells transiently expressing both full-length Tau labeled by EGFP (green) and HA-tagged wild-type PDI with endogenous TIA-1 were also cultured for 1 day, then incubated with 0 (K–O, unstressed) or 500 μM $NaAsO_2$ for 45 min (P–T), fixed, permeabilized, immunostained with the anti-HA antibody (red) and anti-TIA-1 antibody (magenta), stained with DAPI (blue), and observed by confocal microscopy. We have replaced images B, G, L, and Q with better-quality images. White arrows were used to highlight TIA-1-positive stress granules containing Tau in HEK-293T cells (G, H, J, Q, R, and T), and magenta dots indicated TIA-1-positive stress granules formed in HEK-293T cells under stress conditions (H and R). The scale bars represent 10 μm.

Discussion

Recently, Tau has been reported to be able to undergo liquid-liquid phase separation and the subsequent fibril formation [24–34]. This article examines the influence of PDI, acting as a chaperone, on various properties of Tau, including aggregation, toxicity, and fluidity. The modulation of these properties by S-nitrosylation of PDI is also reported. Previous reports have shown that PDI is colocalized with Tau in NFTs, accompanied by a decrease in the expression level of PDI [52,53], but the mechanism behind this phenomenon and the impact of S-nitrosylation of PDI on the pathogenesis of neurodegenerative diseases [48,50–53,74,75] are largely unknown. In the present study, we observed a specific interaction between Tau and wild-type PDI in liquid droplets of Tau and in living cells. One striking observation was that PDI not only significantly inhibited Tau phosphorylation and aggregation in cells but also significantly decreased Tau cytotoxicity resulting from Tau aberrant aggregation. We showed that PDI is recruited by liquid droplets of Tau, which inhibits phase separation and stress granule formation. The phase separation of misfolded proteins is increasingly implicated in neurodegeneration [10–34], and this article raises very interesting questions. We propose that molecular chaperones can be recruited to liquid droplets of Tau to inhibit Tau accumulation in the droplets and that cells are able to use chaperones to prevent the accumulation of misfolded proteins in stress granules. The following experiments support this viewpoint. Transportin 1, a molecular chaperone, has been reported to be recruited to stress granules containing FUS, and increased Transportin 1 expression inhibits FUS accumulation in stress granules [21,22]. HspB8 and Hsp70 have been observed to be specifically recruited into stress granules; these chaperones neutralize misfolded

proteins in aberrant stress granules [20,43]. More importantly, we found that S-nitrosylated PDI, a disease-associated PDI, was excluded from liquid droplets of Tau and relatively immune to interactions with Tau. We propose that aberrant modification of PDI by S-nitrosylation of Cys-312 can abrogate its ability to recognize and recruit targeted proteins.

FRAP can be used to assess the transition of proteins, such as Tau, from a reversible liquid state to a gel-like state of higher viscosity, which is characterized by a decrease in fluorescence recovery rates in the gel state [15,24]. In the present study, when we photobleached Tau droplets formed after the recruitment of wild-type PDI, they recovered rapidly and completely with a fluorescence recovery rate of $(5.67 \pm 0.05) \times 10^{-2}$ s^{-1} or $(3.41 \pm 0.06) \times 10^{-2}$ s^{-1}, which was about 5-fold faster than the recovery rate of $(1.64 \pm 0.05) \times 10^{-2}$ s^{-1} or $(5.37 \pm 0.62) \times 10^{-3}$ s^{-1} before the recruitment, and the latter had a ~10% immobile Tau molecule fraction in the droplets. However, when we photobleached Tau droplets formed in the presence of SNO-PDI, they recovered slowly and incompletely with a fluorescence recovery rate of $(6.04 \pm 0.06) \times 10^{-3}$ s^{-1} or $(3.38 \pm 0.05) \times 10^{-3}$ s^{-1}, which was similar to that before the recruitment, and the former had about 12% immobile Tau molecule fraction in the droplets. We found that liquid droplets of Tau formed after the recruitment of wild-type PDI were much more difficult to be photobleached than those formed before the recruitment or those formed in the presence of SNO-PDI, so that only a small portion of a droplet (about 25%) was bleached. Therefore, we demonstrated that wild-type PDI significantly enhanced the mobility and dynamics of Tau molecules in the droplets, but SNO-PDI did not have remarkable effects on the mobility and dynamics. We also demonstrated that wild-type PDI significantly inhibited the phase transition of Tau from liquids (liquid droplets) to hydrogels, but SNO-PDI did not inhibit such a phase transition. We propose that the recruitment of molecular chaperones, such as Hsp70 and PDI, can significantly enhance the mobility and dynamics of targeted proteins in liquid droplets to maintain the liquidity of membrane-less organelles formed by liquid-liquid

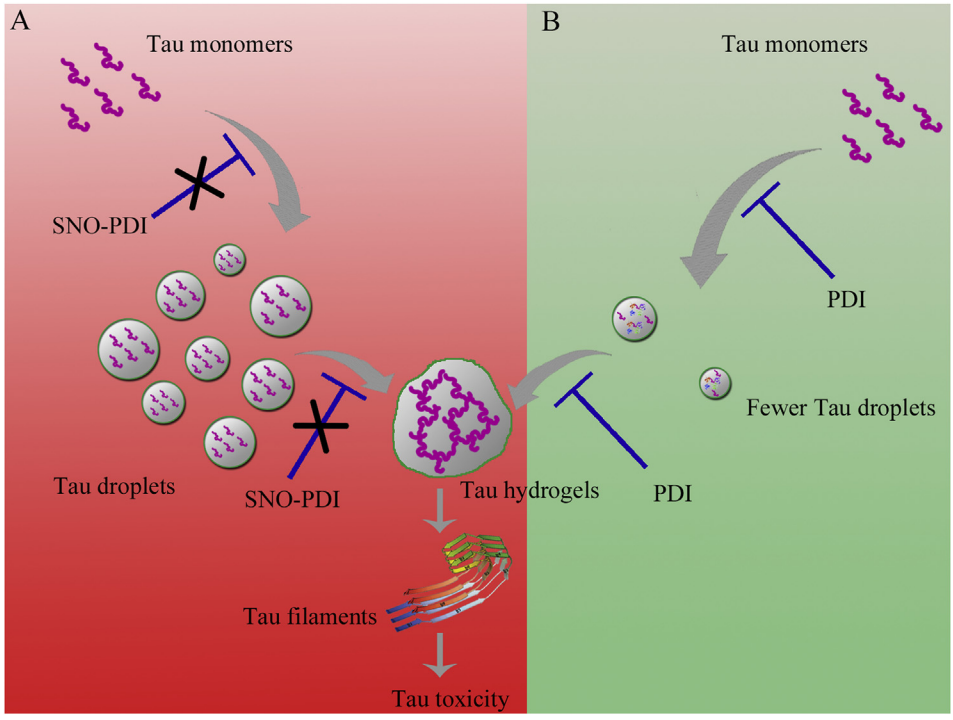

Fig. 10. A hypothetical model shows how PDI and S-nitrosylation of this molecular chaperone modulate phase separation and cytotoxicity of Tau. (B) In the brain of healthy people, wild-type PDI significantly inhibits the phase separation, phase transition, and fibril formation of Tau by acting as a chaperone and significantly decreases Tau cytotoxicity resulting from Tau abnormal aggregation. (B) Much fewer Tau droplets (green balls), hydrogels (green ellipsoids), and filaments (ribbon structure) are formed from Tau monomers (magenta ropes) in the presence of wild-type PDI than in the absence of PDI. (A) In the brain of AD patients, PDI is S-nitrosylated (SNO-PDI), and the S-nitrosylation of this chaperone, not only abrogates its ability to inhibit the phase separation, phase transition, and fibril formation of Tau but also abrogates its ability to decrease Tau cytotoxicity. Much more Tau droplets, hydrogels, and filaments are formed in the presence of SNO-PDI than in the presence of wild-type PDI.

phase separation and to prevent the accumulation of misfolded proteins in the organelles. The following experiments support this viewpoint. The HspB8-BAG3-Hsp70 chaperone complex has been reported to maintain the dynamics of stress granules by preventing defective ribosomal product accumulation inside the granules [43]. Molecular chaperones, including Hsp70, have been observed to be recruited at PML nuclear bodies to maintain the dynamics of PML nuclear bodies by clearing misfolded proteins [76].

The following findings of our study have advanced the field of the phase separation and phase transition of proteins in neurodegenerative diseases [10−15,73]. First, we found that wild-type PDI significantly inhibited not only the phase separation and phase transition of Tau but also the subsequent fibril formation of Tau by acting as a molecular chaperone (Fig. 10B). This finding is confirmed by our demonstration that a specific interaction between Tau and wild-type PDI resulted in the recruitment of this chaperone into Tau droplets that significantly inhibited not only the liquid-liquid phase separation of Tau but also the formation of the β-sheet conformation of Tau droplets. This finding is also confirmed by our demonstration that much fewer Tau droplets, hydrogels, and filaments were formed in the presence of wild-type PDI than in the absence of PDI (Fig. 10B). Second, we revealed that Tau after the recruitment of wild-type PDI had significantly weaker aggregation ability in cells than that before the recruitment and protected against mitochondrial damage in cells caused by Tau aggregation. Third, we observed that wild-type PDI significantly decreased Tau aggregation-induced apoptosis and cytotoxicity (Fig. 10). Mitochondrial damage and Tau cytotoxicity are key functional consequences of liquid-liquid phase separation and aggregation of Tau. Tau aggregation under pathological conditions causes mitochondrial damage in cells, and mitochondrial dysfunction further enhances Tau aggregation in cells, and finally causes Tau cytotoxicity. Finally, we showed that S-nitrosylation of PDI not only abrogated its ability to inhibit the phase separation, phase transition, and fibril formation of Tau but also abrogated its ability to decrease Tau cytotoxicity (Fig. 10A). This finding is supported by our demonstration that much more Tau droplets, hydrogels, and filaments were formed in the presence of SNO-PDI than in the presence of wild-type PDI (Fig. 10). Our study enhances our understanding of how molecular chaperones regulate the phase separation, phase transition, and cytotoxicity of Tau and helps explain the mechanism underlying the very interesting protective effect of molecular chaperones against Tau toxicity in AD and related neurodegenerative diseases observed in humans and animal models. Our study also enhances our understanding of how S-nitrosation of PDI, a perturbation in this regulation, leads to disease.

Materials and Methods

Materials

ATTO 647, three dyes, Congo red (fresh molecular weight of 696.67), ThT, and DAPI, and two antibodies, the mouse/rabbit anti-HA monoclonal antibody, and mouse anti-β-actin antibody, were purchased from Sigma-Aldrich (St. Louis, MO). The mouse anti-Tau monoclonal antibody Tau-5, rabbit anti-pS396 monoclonal antibody, and ER Staining Kit (ab139482) were obtained from Abcam (Cambridge, UK). All Alexa-conjugated fluorescent secondary antibodies were purchased from Beyotime (Nantong, China). Sarkosyl was purchased from Amresco (Solon, OH). Ni-Sepharose and SP-Sepharose Fast Flow were purchased from GE Company (Pittsburgh, PA). All other chemicals used in this study were of analytical grade and were produced in China.

Protein purification

A plasmid-encoding human Tau40 was a kind gift from Dr. Michel Goedert (University of Cambridge). A pathogenic mutation ΔK280 of $Tau_{244-372}$, the microtubule-binding region of Tau, was subcloned into a prokaryotic expression vector pRK172. The construction of prokaryotic plasmids expressing ΔK280 and the purification of Tau were carried as described in detail previously [2,3,59,60]. Purified Tau was analyzed by sodium dodecyl sulfate-polyacrylamide gel electrophoresis (SDS-PAGE) with one band. The concentration of Tau was determined according to its absorbance at 214 nm with a standard calibration curve drawn by BSA.

A plasmid-encoding human PDI was a kind gift from Dr. Lloyd W. Ruddock (University of Oulu). The recombinant wild-type full-length human PDI was constructed into a prokaryotic expression vector pET28 and expressed in *E. coli* BL21 (DE3) Codon plus-RIL cells (Novagen, Merck, Darmstadt, Germany). Cells were harvested by centrifugation (12,000 *g* for 5 min) and resuspended in 100 ml buffer A (20 mM Na_3PO_4 and 1 mM PMSF, pH 7.3). The cell suspension was lysed by ultrasonication for 30 min, then add 1 g streptomycin sulfate into the cell lysate and wait for 2 h at 4 °C to remove DNA. After loading, the column was washed by 100 ml buffer B (20 mM Na_3PO_4, 500 mM NaCl, and 50 mM imidazole, pH 7.3) to remove proteins with low affinities to a Ni^{2+} affinity column, and then buffer A was used to equilibrate the column. Finally, the protein was eluted with 200 ml buffer C (20 mM

Na_3PO_4 and 50 mM EDTA, pH 7.0). The eluted fractions were dialyzed into the HEPES buffer twice to remove EDTA. Purified PDI was analyzed by SDS-PAGE with one band. The concentration of PDI was determined according to its absorbance at 214 nm with a standard calibration curve drawn by BSA.

A plasmid containing human HSP70 gene was a kind gift from Dr. Sonia Longhi (Aix-Marseille University, CNRS). Wild-type full-length human Hsp70 was subcloned into a prokaryotic expression vector pDEST14, and Hsp70 production was carried out in *E. coli* BL21 (DE3) Codon plus-RIL cells (Novagen, Merck, Darmstadt, Germany). Cells were harvested by centrifugation (12,000 *g* for 5 min) and resuspended in 100 ml buffer D (20 mM Na_3PO_4, 300 mM NaCl, 10 mM imidazole, and 1 mM PMSF, pH 8.0). The cell suspension was lysed by ultrasonication for 30 min, then add 1 g streptomycin sulfate into the cell lysate and wait for 2 h at 4 °C to remove DNA. The cell debris was removed by centrifugation at 17,000 *g* for 30 min. The supernatant was filtered through a 0.45 μm filter and then applied to a Ni^{2+} affinity column at a flow rate of 1 ml/min. After loading, the column was washed by 50 ml buffer E (20 mM Na_3PO_4, 300 mM NaCl, and 30 mM imidazole, pH 8.0) to remove proteins with low affinities to a Ni^{2+} affinity column, and then buffer D was used to equilibrate the column. Finally, the protein was eluted with 30 ml buffer F (20 mM Na_3PO_4, 300 mM NaCl, and 250 mM imidazole, pH 8.0). The eluted fractions were dialyzed into HEPES buffer twice to remove imidazole. Purified Hsp70 was analyzed by SDS-PAGE with one band. We used a NanoDrop OneC Microvolume UV−Vis Spectrophotometer (Thermo Scientific, Waltham, MA) to determine the concentration of Hsp70 using its absorbance at 280 nm and molar extinction coefficient calculated from the composition of the protein (http://web.expasy.org/protparam/).

S-nitrosocysteine synthesis and production of S-nitrosylated PDI

S-nitrosocysteine was synthesized as described in detail below. Cysteine was dissolved in 0.625 M HCl at 0 °C to a final concentration of 625 mM. An equimolar amount of $NaNO_2$ was added and the mixture was stirred at 0 °C for 40 min. A 2.5-fold volume of acetone was then added, and the new mixture was stirred at 0 °C for 20 min, followed by filtration of the precipitate. S-nitrosocysteine was washed once with 80% acetone, twice with 100% acetone, three times with diethyl ether, and finally, was freeze-dried.

S-nitrosylated PDI (SNO-PDI) was produced by the reaction of wild-type PDI with the physiological NO donor S-nitrosocysteine. To produce SNO-PDI, wild-type PDI and S-nitrosocysteine were cultured at a molar ratio of 1:100 and incubated for 30 min at room temperature, then concentrated the protein and washed with 10 mM HEPES buffer (pH 7.4) containing 100 mM NaCl to remove residual S-nitrosocysteine, using centrifugal filters.

Nano-LC-MS/MS analysis

All nano-LC-MS/MS experiments were performed on a Q Exactive LC-MS/MS System (Thermo Scientific, Waltham, MA) equipped with an Easy *n*-LC 1000 HPLC system (Thermo Scientific). The IodoTMT reagent-labeled peptides were loaded onto a 100 μm id × 2 cm fused silica trap column packed in-house with reversed-phase silica (Reprosil-Pur C18 AQ, 5 μm, Dr. Maisch GmbH) and then separated on a 75 μm id × 20 cm C18 column packed with reversed-phase silica (Reprosil-Pur C18 AQ, 3 μm, Dr. Maisch GmbH). The peptides bounded on the column were eluted with a 75-min linear gradient. The solvent A consisted of 0.1% formic acid in water solution, and the solvent B consisted of 0.1% formic acid in acetonitrile solution. The segmented gradient was 4−12% B, 5 min; 12−22% B, 50 min; 22−32% B, 12 min; 32−90% B, 1 min; 90% B, 7 min at a flow rate of 300 nl/min.

The MS analysis was performed with Q Exactive mass spectrometer (Thermo Scientific). With the data-dependent acquisition mode, the MS data were acquired at a high resolution of 70,000 (*m/z* 200) across the mass range of 300−1600 *m/z*. The target value was 3e6, with a maximum injection time of 60 ms. The top 20 precursor ions were selected from each MS full scan with an isolation width of 2 *m/z* for fragmentation in the HCD collision cell with a normalized collision energy of 27%. Subsequently, MS/MS spectra were acquired at a resolution of 17,500 at *m/z* 200. The target value was 5e4, with a maximum injection time of 80 ms. The dynamic exclusion time was 40 s. For nanoelectrospray ion source setting, the spray voltage was 2.0 kV; no sheath gas flow; the heated capillary temperature was 320 °C.

The raw data from Q Exactive were analyzed with Proteome Discovery version 1.4 using the Sequest HT search engine for protein identification and Percolator for FDR (false discovery rate) analysis against a Uniprot human protein database (updated on September 2018). Some important searching parameters were set as following: trypsin was selected as an enzyme and two missed cleavages were allowed for searching; the mass tolerance of precursor was set as 10 ppm, and the product ion's tolerance was 0.02 Da; cysteine carbamidomethylation, methionine oxidation, MMTS and iodoTMT6-plex on cysteine were selected as variable modifications. FDR analysis was performed with Percolator, and FDR <1% was set for protein

identification. The peptide's confidence was set as high for peptides filter.

Liquid-droplet and hydrogel formation

The freshly purified ΔK280 of $Tau_{244-372}$ was incubated with TAMRA (red fluorescence) at a Tau:TAMRA molar ratio of 1:3 for 1 h, the freshly purified wild-type PDI was incubated with ATTO 647 (green fluorescence) at a PDI: ATTO molar ratio of 1:3 for 1 h, and the freshly purified SNO-PDI, Hsp70, and BSA were incubated with FITC (green fluorescence) at a protein:FITC molar ratio of 1:3 for 1 h. These labeled proteins were filtered and freeze-dried. 100 μM ΔK280 labeled by TAMRA was incubated with 10 mM HEPES buffer (pH 7.4) containing 100 mM NaCl, 25 μM heparin, and 12.5% Ficoll 70 or incubated with the same buffer further containing 100 μM wild-type PDI labeled by ATTO 647 or 100 μM SNO-PDI labeled by FITC or 100 μM Hsp70 labeled by FITC or 100 μM BSA labeled by FITC on ice to induce liquid-liquid phase separation for 30 min and hydrogel formation for 10 days. Images of 10-μl samples were captured using a Leica TCS SP8 laser scanning confocal microscope (Wetzlar, Germany), and liquid droplets of 100 μM ΔK280 in HEPES were observed by DIC confocal microscopy, with excitation at 546 nm. Hydrogels of 100 μM ΔK280 in HEPES were observed using a Leica DMi8 inverted microscope (Wetzlar, Germany) with a red fluorescence filter. ΔK280 in liquids was stained with ThT (cyan fluorescence), and liquid droplets of ΔK280 were observed by DIC confocal microscopy, with excitation at 440 nm. Liquid droplets of ΔK280 formed after the recruitment of wild-type PDI were also observed by DIC confocal microscopy, with excitation at 647 nm. Liquid droplets of ΔK280 formed in the presence of SNO-PDI or Hsp70 or BSA were also observed by DIC confocal microscopy, with excitation at 488 nm. Hsp70 and BSA were used as a positive control and negative control, respectively. Wild-type PDI labeled by ATTO 647 incubated with 10 mM HEPES buffer (pH 7.4) containing 100 mM NaCl, 25 μM heparin, and 12.5% Ficoll 70 on ice for 30 min were used as a control. Neither phase separation nor ThT staining for 100 μM wild-type PDI in HEPES was observed by DIC confocal microscopy with excitation at 647 nm and 440 nm, respectively. Sucrose was used as a control for Ficoll 70. ΔK280 labeled by TAMRA incubated with 10 mM HEPES buffer (pH 7.4) containing 100 mM NaCl, 25 μM heparin, and 12.5% sucrose or incubated with HEPES containing 100 mM NaCl, 12.5% Ficoll 70, and no heparin, on ice for 30 min were used as controls. No phase separation for 100 μM ΔK280 in either HEPES buffer was observed by DIC confocal microscopy, with excitation at 546 nm.

Fluorescence recovery after photobleaching

100 μM ΔK280 labeled by TAMRA was incubated with 10 mM HEPES buffer (pH 7.4) containing 100 mM NaCl, 25 μM heparin, and 12.5% Ficoll 70 or incubated with the same buffer further containing 100 μM wild-type PDI labeled by ATTO 647 or 100 μM SNO-PDI labeled by FITC on ice to induce liquid-liquid phase separation for 30 min. FRAP measurements were performed using a Leica TCS SP8 laser scanning confocal microscope (Wetzlar, Germany) with excitation at 546 nm. Droplets of a size of ~4 μm, 1−2 μm, and ~3 μm were selected for ΔK280 before the recruitment of wild-type PDI, after the recruitment, and in the presence of SNO-PDI, respectively. For each droplet, a square was bleached at 80% transmission for 25 flashes (3 s per flash), and postbleaching time-lapse images were collected (50 frames, 5 s per frame). Images were analyzed using Leica LAS AF Lite.

Cell culture and transfection

HEK-293T and SH-SY5Y cells were cultured in minimum essential media and in Dulbecco's modified Eagle's medium (Gibco, Invitrogen, Mulgrave, VIC, Australia), respectively, supplemented with 10% (v/v) fetal bovine serum (Gibco), 100 U/ml streptomycin, and 100 U/ml penicillin in 5% CO_2 at 37 °C. HEK-293T and SH-SY5Y cell line stably expressing wild-type full-length human Tau or its pathogenic mutation ΔK280, was constructed with a lentiviral vector construction system (pHAGE-puro). The target DNA fragments were inserted into the lentiviral vector, and the plasmids containing target DNA, pVSVG, and p976 were packaged in HEK-293T cells at a ratio of 2:1:1 by Lipofectamine® 2000 (Invitrogen, Carlsbad, CA). The ratio of liposome to DNA was 2:1. After 48 h of transfection, the viruses were harvested and filtered, and then HEK-293T and SH-SY5Y cells were infected with the packaged lentivirus twice for 12 h each with a 12-h interval. In order to establish the stable cell lines, puromycin was used to screen overexpressed cells. The expression of each protein was detected by Western blot.

Sarkosyl-insoluble Western blotting

SH-SY5Y cells stably expressing full-length Tau or its pathogenic mutation ΔK280 were cultured in 6-well plates for 2 days. These cells were then transiently expressed HA-tagged wild-type PDI or HA-tagged dnPDI and incubated with 10 μM Congo red, or transfected with empty vector and directly incubated with 10 μM Congo red. After 3 days, cells were harvested and ruptured on ice for 15 min with RIPA lysis buffer containing 50 mM Tris (pH 7.4), 150 mM NaCl, 1% NP-40, 0.5% sodium

deoxycholate, 0.1% SDS, EDTA, and leupeptin (Beyotime). The cell lysates were boiled in SDS-PAGE loading buffer for 15 min, then subjected to 12.5% SDS-PAGE and transferred to polyvinylidene difluoride membranes (Millipore). The membranes were blocked with 5% fat-free milk in 25 mM Tris-buffered saline buffer containing 0.047% Tween 20 (TBST) and then incubated with 1/1000 the rabbit anti-pS396 antibody, rabbit anti-HA antibody, and rabbit anti-β-actin antibodies separately for 1 h at room temperature, followed by incubation with 1/10,000 homologous horseradish peroxidase (HRP)-conjugated secondary antibody for 1 h at room temperature. The membranes were then incubated with WesternBright ECL HRP substrate (Advansta Inc., Menlo Park, CA) and developed on films. The normalized amount of pS396 Tau or pS396 ΔK280 in SH-SY5Y cells stably expressing full-length Tau or ΔK280 and transiently expressing PDI was determined as a ratio of the density of pS396 Tau bands or pS396 ΔK280 bands over the density of β-actin band in the cell lysates. SH-SY5Y cells stably expressing full-length Tau or ΔK280 were used as a control. The cell lysates were centrifuged at 17,000 *g* for half an hour at 4°C to remove the cell debris. Half of the supernatant was incubated with 1% sarkosyl for half an hour at 25°C. The mixture was then ultracentrifuged at 150,000 *g* for half an hour, and the pellets were washed twice with 1 × PBS (pH 7.4). The sarkosyl-insoluble pellets were boiled in the SDS-PAGE loading buffer for 15 min. The other half of the supernatant, which served as the total protein sample, was also boiled in the SDS-PAGE loading buffer for 15 min. The samples were separated by 12.5% SDS-PAGE, and then Western blotted as described in detail in the aforementioned Tau phosphorylation experiments. The sarkosyl-insoluble pellets from those cells were probed using an anti-Tau antibody Tau-5, and the corresponding cell lysates were probed using Tau-5, the anti-HA antibody, and anti-β-actin antibody. The amount of loaded protein was normalized using a BCA Protein Quantification kit (Beyotime). For calculating the amounts of sarkosyl-insoluble Tau or pS396 Tau, the ImageJ software (NIH, Bethesda, MD) was used to assess the densitometry of Tau bands. The normalized amount of insoluble Tau aggregates in SH-SY5Y cells stably expressing full-length Tau or ΔK280 and transiently expressing PDI was determined as a ratio of the density of insoluble Tau aggregate bands after sample ultracentrifugation over that of the total Tau bands in cell lysates. SH-SY5Y cells stably expressing full-length Tau or ΔK280 were used as the control. The normalized amounts of pS396 Tau or insoluble Tau aggregates are expressed as mean ± S.D. (with error bars) of values obtained in 3 independent experiments. Statistical analyses were performed using the Student *t*-test. Values of $p < 0.05$ indicate statistically significant differences. The following notation is used throughout: *, $p < 0.05$; **, $p < 0.01$; and ***, $p < 0.001$ relative to full-length Tau or its pathogenic mutation ΔK280 in the absence of PDI.

Laser scanning confocal analysis

SH-SY5Y cells stably expressing full-length Tau or its pathogenic mutation ΔK280 were cultured for 2 day, then transiently expressed HA-tagged wild-type PDI or HA-tagged dnPDI and incubated with 10 μM Congo red for 3 days at 37 °C, or directly incubated with 10 μM Congo red for 3 days at 37 °C, fixed, permeabilized, immunostained with the rabbit anti-pS396 monoclonal antibody and IgG conjugated to Alexa Fluor 488 (green) and with the mouse anti-HA monoclonal antibody and IgG conjugated to Alexa Fluor 555 (red), and stained with DAPI (blue). Images were captured using a Leica TCS SP8 laser scanning confocal microscope (Wetzlar, Germany).

BiFC

The human Tau40 gene was cloned into the pEGFP n1 by Mlu I and BamH I restriction sites. The fusion gene was truncated at amino acid 172 of EGFP using a stop codon, and then full-length Tau-$EGFP_{1\text{-}172}$ was obtained. The human Tau40 gene was cloned into the pcDNA 3.1 vector by Xba I and Kpn I restriction sites. The fused HA-tag and $EGFP_{155\text{-}238}$ genes were inserted into the PDI genes between the signal peptide and the amino acid coding sequence, then HA-tagged $EGFP_{155\text{-}238}$-wild-type PDI was obtained. We mutated the four cysteines of $EGFP_{155\text{-}238}$-wild-type PDI to alanine to obtain $EGFP_{155\text{-}238}$-dnPDI. The fusion proteins were detected by Western blot. One day before transfection, HEK-293T cells were plated on glass-bottom culture dishes, and then the cells were transiently cotransfected with pEGFP-Tau-$EGFP_{1\text{-}172}$ and pcDNA 3.1-$EGFP_{155\text{-}238}$-PDI according to the manufacturer's instructions. Living HEK-293T cells, transiently expressing both Tau-$EGFP_{1\text{-}172}$ and $EGFP_{155\text{-}238}$-wild-type PDI or $EGFP_{155\text{-}238}$-dnPDI constructs, were cultured for 1 day, and then stained with CytoPainter ER Staining Kit (red) following the instructions. Images were captured using a Leica TCS SP8 laser scanning confocal microscope (Wetzlar, Germany). Confocal microscopy was also used to visualize the fluorescence of the following control cells: living HEK-293T cells transiently expressing both $EGFP_{1\text{-}172}$ and $EGFP_{155\text{-}238}$-PDI, or $EGFP_{155\text{-}238}$-dnPDI or $EGFP_{155\text{-}238}$ constructs or living cells transiently expressing both Tau-$EGFP_{1\text{-}172}$ and $EGFP_{155\text{-}238}$ constructs.

Ultrathin TEM

HEK-293T cells stably expressing ΔK280 of full-length Tau were cultured for 2 days, then transiently expressed HA-tagged wild-type PDI or HA-tagged dnPDI and incubated with 5 μM Tau oligomers for 2 days. Tau oligomers were formed when full-length Tau (10 μM) was incubated with 10 mM HEPES buffer (pH 7.4) containing 100 mM NaCl, 2.5 μM heparin and 1 mM DTT and at 37 °C for 1.5 h. HEK-293T cells stably expressing ΔK280 and directly incubated with 5 μM Tau oligomers for 2 days and cells transfected with empty vector and incubated with HEPES buffer were used as a negative control and positive control, respectively. After prefixation with 3% paraformaldehyde and 1.5% glutaraldehyde in 1 × PBS (pH 7.4), the cells were harvested and postfixed in 1% osmium tetroxide for 1 h using an ice bath; the samples were then dehydrated in graded acetone and embedded in 812 resins. Ultrathin sections of the cells were prepared using a Leica Ultracut S Microtome (Buffalo Grove, IL) and negatively stained using 2% uranyl acetate and lead citrate. The doubly stained ultrathin sections of cells were examined using a JEM-1400 Plus transmission electron microscope (JEOL) operating at 100 kV.

Annexin V-FITC apoptosis detection assay

SH-SY5Y and HEK-293T cells stably expressing ΔK280 of full-length Tau were cultured for 2 days, then transiently expressed HA-tagged wild-type PDI or HA-tagged dnPDI and incubated with 5 μM Tau oligomers for 2 days. SH-SY5Y and HEK-293T cells stably expressing ΔK280 and directly incubated with 5 μM Tau oligomers for 2 days were used as negative controls. Apoptotic cells were detected by flow cytometry after staining with an annexin V-FITC apoptosis detection kit (Beyotime). In brief, SH-SY5Y cells were harvested after digestion with 2.5 mg/ml trypsin (Promega, Madison, WI) and HEK-293T cells were directly harvested; the cells were washed twice with 1 × PBS at 4 °C and resuspended in 185 μl of binding buffer. The samples were then incubated with 5 μl of annexin V-FITC and 10 μl of PI for 15 min at 4 °C in the dark. Annexin V binding was analyzed using an EPICS XL-MCL flow cytometer (Beckman Coulter, Fullerton, CA), and the percentage of apoptotic cells was calculated from the total number of cells (~3×10^{-4} cells) as described in detail previously [60]. All apoptotic blot experiments were repeated three times.

Stress granule formation

HEK-293T cells transiently expressing both full-length Tau labeled by EGFP and HA-tagged wild-type PDI with endogenous TIA-1 were cultured for 1 day, and then incubated with 0 or 500 μM $NaAsO_2$ for 45 min at 37 °C. HEK-293T cells transiently expressing full-length Tau labeled by EGFP with endogenous TIA-1 also cultured for 1 day and then incubated with 0 or 500 μM sodium arsenite for 45 min were used as the control. Cells were fixed with 4% paraformaldehyde for 30 min, followed by lysed in 0.25% Triton X-100 and blocked with 5% BSA at 37 °C, then coimmunostained with the rabbit anti-TIA-1 antibody and the mouse anti-HA antibody, stained with DAPI (blue), and finally incubated with Alexa Fluo labeled secondary antibody. Images were captured using a Leica TCS SP8 laser scanning confocal microscope (Wetzlar, Germany).

Statistical analysis

The data shown for each experiment were based on at least three technical replicates, as indicated in individual figure legends. Data are presented as mean ± S.D., and *p*-values were determined using the Student *t*-test. All experiments were further confirmed by biological repeats.

Acknowledgments

We sincerely thank Dr. Michel Goedert (University of Cambridge), Dr. Lloyd W. Ruddock (University of Oulu), and Dr. Sonia Longhi (Aix-Marseille University, CNRS) for the kind gifts of the human Tau40 plasmid, the human PDI plasmid, a plasmid containing the human HSP70 gene, respectively. We thank Dr. Zhiyin Song for his technical assistance with the TEM of ultrathin sections of cells, and Dr. Jifeng Wang and Dr. Zhensheng Xie (Institute of Biophysics, Chinese Academy of Sciences) for their technical assistance with nano-LC-MS/MS. This work was supported by the National Natural Science Foundation of China Grants 31770833, 31570779, 31370774, 91849203, and 31570857, the National Key Basic Research Foundation of China Grants 2013CB910702, 2012CB911003, and 2017YFA0504000 and the Fundamental Research Fund for the Central Universities of China 2015204020201.

Author contributions

Kan Wang: Conceptualization, Methodology, Validation, Investigation, Writing- Original draft preparation, Visualization; Jia-Qi Liu: Conceptualization, Methodology, Validation, Investigation; Tao Zhong: Methodology, Validation, Investigation; Xiao-Ling Liu: Methodology, Investigation; Yan Zeng: Data

curation, Investigation; Xinhua Qiao: Formal analysis, Methodology; Ting Xie: Methodology, Investigation; Yuzhe Chen: Methodology, Investigation; Ying-Ying Gao: Methodology, Software; Bo Tang: Methodology, Investigation; Jia Li: Methodology, Validation; Jun Zhou: Resources; Dai-Wen Pang: Resources; Jie Chen: Project administration; Chang Chen: Conceptualization, Methodology, Funding acquisition; Yi Liang: Conceptualization, Methodology, Validation, Investigation, Writing- Original draft preparation, Supervision, Writing-Reviewing and Editing, Project administration, Funding acquisition.

Conflict of interest statement

The authors declare no competing financial interests.

Appendix A. Supplementary data

Supplementary data to this article can be found online at https://doi.org/10.1016/j.jmb.2020.02.013.

Received 24 September 2019;
Received in revised form 21 January 2020;
Accepted 11 February 2020
Available online 19 February 2020

Keywords:
molecular chaperone;
protein phase separation;
protein disulfide isomerase;
Tau protein;
protein aggregation

†K.W. and J.-Q.L. contributed equally to this work.

Abbreviations used:
PDI, protein disulfide isomerase; AD, Alzheimer's disease; SNO, S-nitrosylated; ER, endoplasmic reticulum; BiFC, bimolecular fluorescence complementation; DAPI, 4′,6-diamidino-2-phenylindole dihydrochloride; DIC, differential interference contrast; PI, propidium iodide; TAMRA, 5(6)-carboxy-tetramethylrhodamine N-succinimidyl ester; FRAP, fluorescence recovery after photobleaching; TIA-1, T cell intracellular antigen-1; ThT, thioflavin T; DTT, dithiothreitol; TEM, transmission electron microscopy; PMSF, phenylmethanesulfonyl fluoride.

References

[1] M.D. Mukrasch, S. Bibow, J. Korukottu, S. Jeganathan, J. Biernat, C. Griesinger, et al., Structural polymorphism of 441-residue Tau at single residue resolution, PLoS Biol. 7 (2) (2009) e1000034.
[2] Z.Y. Mo, Y.Z. Zhu, H.L. Zhu, J.B. Fan, J. Chen, Y. Liang, Low micromolar zinc accelerates the fibrillization of human Tau via bridging of Cys-291 and Cys-322, J. Biol. Chem. 284 (50) (2009) 34648–34657.
[3] H.L. Zhu, C. Fernandez, J.B. Fan, F. Shewmaker, J. Chen, A.P. Minton, et al., Quantitative characterization of heparin binding to Tau protein: implication for inducer-mediated Tau filament formation, J. Biol. Chem. 285 (6) (2010) 3592–3599.
[4] Y. Wang, E Mandelkow, Tau in physiology and pathology, Nat. Rev. Neurosci. 17 (1) (2016) 5–21.
[5] T. Guo, W. Noble, D.P. Hanger, Roles of Tau protein in health and disease, Acta Neuropathol. 133 (5) (2017) 665–704.
[6] E.H. Kellogg, N.M.A. Hejab, S. Poepsel, K.H. Downing, F. DiMaio, E. Nogales, Near-atomic model of microtubule-Tau interactions, Science 360 (6394) (2018) 1242–1246.
[7] C. Ballatore, V.M. Lee, J.Q. Trojanowski, Tau-mediated neurodegeneration in Alzheimer's disease and related disorders, Nat. Rev. Neurosci. 8 (9) (2007) 663–672.
[8] E.M. Mandelkow, E. Mandelkow, Biochemistry and cell biology of Tau protein in neurofibrillary degeneration, Cold Spring Harb. Perspect. Med. 2 (7) (2012) a006247.
[9] K. Zhou, C. Yuan, B. Dai, K. Wang, Y. Chen, D. Ma, et al., Environment-sensitive near-infrared probe for fluorescent discrimination of Aβ and Tau fibrils in AD brain, J. Med. Chem. 62 (14) (2019) 6694–6704.
[10] Y. Shin, C.P. Brangwynne, Liquid phase condensation in cell physiology and disease, Science 357 (6357) (2017), eaaf4382.
[11] V.N. Uversky, Protein intrinsic disorder-based liquid-liquid phase transitions in biological systems: complex coacervates and membrane-less organelles, Adv. Colloid Interface Sci. 239 (2017) 97–114.
[12] S. Boeynaems, S. Alberti, N.L. Fawzi, T. Mittag, M. Polymenidou, F. Rousseau, et al., Protein phase separation: a new phase in cell biology, Trends Cell Biol. 28 (6) (2018) 420–435.
[13] Z. Wang, H. Zhang, Phase separation, transition, and autophagic degradation of proteins in development and pathogenesis, Trends Cell Biol. 29 (5) (2019) 417–427.
[14] N.B. Nedelsky, J.P. Taylor, Bridging biophysics and neurology: aberrant phase transitions in neurodegenerative disease, Nat. Rev. Neurol. 15 (5) (2019) 272–286.
[15] S. Elbaum-Garfinkle, Matter over mind: liquid phase separation and neurodegeneration, J. Biol. Chem. 294 (18) (2019) 7160–7168.
[16] A. Patel, H.O. Lee, L. Jawerth, S. Maharana, M. Jahnel, M.Y. Hein, et al., A liquid-to-solid phase transition of the ALS protein FUS accelerated by disease mutation, Cell 162 (5) (2015) 1066–1077.
[17] A. Molliex, J. Temirov, J. Lee, M. Coughlin, A.P. Kanagaraj, H.J. Kim, et al., Phase separation by low complexity domains promotes stress granule assembly and drives pathological fibrillization, Cell 163 (1) (2015) 123–133.
[18] S. Xiang, M. Kato, L.C. Wu, Y. Lin, M. Ding, Y. Zhang, et al., The LC domain of hnRNPA2 adopts similar conformations in hydrogel polymers, liquid-like droplets, and nuclei, Cell 163 (4) (2015) 829–839.
[19] Z. Monahan, V.H. Ryan, A.M. Janke, K.A. Burke, S.N. Rhoads, G.H. Zerze, et al., Phosphorylation of the FUS low-complexity domain disrupts phase separation,

aggregation, and toxicity, EMBO J. 36 (20) (2017) 2951–2967.
[20] D. Mateju, T.M. Franzmann, A. Patel, A. Kopach, E.E. Boczek, S. Maharana, et al., An aberrant phase transition of stress granules triggered by misfolded protein and prevented by chaperone function, EMBO J. 36 (12) (2017) 1669–1687.
[21] L. Guo, H.J. Kim, H. Wang, J. Monaghan, F. Freyermuth, J.C. Sung, et al., Nuclear-import receptors reverse aberrant phase transitions of RNA-binding proteins with prion-like domains, Cell 173 (3) (2018) 677–692.
[22] M. Hofweber, S. Hutten, B. Bourgeois, E. Spreitzer, A. Niedner-Boblenz, M. Schifferer, et al., Phase separation of FUS is suppressed by its nuclear import receptor and arginine methylation, Cell 173 (3) (2018) 706–719.
[23] S. Qamar, G. Wang, S.J. Randle, F.S. Ruggeri, J.A. Varela, J.Q. Lin, et al., FUS phase separation is modulated by a molecular chaperone and methylation of arginine cation-π interactions, Cell 173 (3) (2018) 720–734.
[24] S. Wegmann, B. Eftekharzadeh, K. Tepper, K.M. Zoltowska, R.E. Bennett, S. Dujardin, et al., Tau protein liquid-liquid phase separation can initiate Tau aggregation, EMBO J. 37 (7) (2018) e98049.
[25] S. Boyko, X. Qi, T.H. Chen, K. Surewicz, W.K. Surewicz, Liquid-liquid phase separation of Tau protein: the crucial role of electrostatic interactions, J. Biol. Chem. 294 (29) (2019) 11054–11059.
[26] S. Ambadipudi, J. Biernat, D. Riedel, E. Mandelkow, M. Zweckstetter, Liquid-liquid phase separation of the microtubule-binding repeats of the Alzheimer-related protein Tau, Nat. Commun. 8 (1) (2017) 275.
[27] Y. Lin, J. McCarty, J.N. Rauch, K.T. Delaney, K.S. Kosik, G.H. Fredrickson, et al., Narrow equilibrium window for complex coacervation of Tau and RNA under cellular conditions, eLife 8 (2019) e42571.
[28] J.C. Ferreon, A. Jain, K.J. Choi, P.S. Tsoi, K.R. MacKenzie, S.Y. Jung, et al., Acetylation disfavors Tau phase separation, Int. J. Mol. Sci. 19 (5) (2018) E1360.
[29] J.S. Rane, A. Kumari, D. Panda, An acetylation mimicking mutation, K274Q, in Tau imparts neurotoxicity by enhancing Tau aggregation and inhibiting tubulin polymerization, Biochem. J. 476 (10) (2019) 1401–1417.
[30] T. Ukmar-Godec, S. Hutten, M.P. Grieshop, N. Rezaei-Ghaleh, M.S. Cima-Omori, J. Biernat, et al., Lysine/RNA-interactions drive and regulate biomolecular condensation, Nat. Commun. 10 (1) (2019) 2909.
[31] X. Zhang, Y. Lin, N.A. Eschmann, H. Zhou, J.N. Rauch, I. Hernandez, et al., RNA stores Tau reversibly in complex coacervates, PLoS Biol. 15 (7) (2017) e2002183.
[32] A. Hernández-Vega, M. Braun, L. Scharrel, M. Jahnel, S. Wegmann, B.T. Hyman, et al., Local nucleation of microtubule bundles through tubulin concentration into a condensed Tau phase, Cell Rep. 20 (10) (2017) 2304–2312.
[33] S. Ambadipudi, J.G. Reddy, J. Biernat, E. Mandelkow, M. Zweckstetter, Residue-specific identification of phase separation hot spots of Alzheimer's-related protein Tau, Chem. Sci. 10 (26) (2019) 6503–6507.
[34] A. Majumdar, P. Dogra, S. Maity, S. Mukhopadhyay, Liquid-liquid phase separation is driven by large-scale conformational unwinding and fluctuations of intrinsically disordered protein molecules, J. Phys. Chem. Lett. 10 (14) (2019) 3929–3936.
[35] J.M. Silva, S. Rodrigues, B. Sampaio-Marques, P. Gomes, A. Neves-Carvalho, C. Dioli, et al., Dysregulation of autophagy and stress granule-related proteins in stress-driven Tau pathology, Cell Death Differ. 26 (8) (2019) 1411–1427.
[36] L. Ellgaard, M. Molinari, A. Helenius, Setting the standards: quality control in the secretory pathway, Science 286 (5446) (1999) 1882–1888.
[37] S. Wickner, M.R. Maurizi, S. Gottesman, Posttranslational quality control: folding, refolding, and degrading proteins, Science 286 (5446) (1999) 1888–1893.
[38] F.U. Hartl, A. Bracher, M. Hayer-Hartl, Molecular chaperones in protein folding and proteostasis, Nature 475 (7356) (2011) 324–332.
[39] E.M. Sontag, R.S. Samant, J. Frydman, Mechanisms and functions of spatial protein quality control, Annu. Rev. Biochem. 86 (2017) 97–122.
[40] C. Scheckel, A. Aguzzi, Prions, prionoids and protein misfolding disorders, Nat. Rev. Genet. 19 (7) (2018) 405–418.
[41] S. Thapa, B. Abdulrahman, D.H. Abdelaziz, L. Lu, M. Ben Aissa, H.M. Schatzl, Overexpression of quality control proteins reduces prion conversion in prion-infected cells, J. Biol. Chem. 293 (41) (2018) 16069–16082.
[42] F. Frottin, F. Schueder, S. Tiwary, R. Gupta, R. Körner, T. Schlichthaerle, et al., The nucleolus functions as a phase-separated protein quality control compartment, Science 365 (6451) (2019) 342–347.
[43] M. Ganassi, D. Mateju, I. Bigi, L. Mediani, I. Poser, H.O. Lee, et al., A surveillance function of the HSPB8-BAG3-HSP70 chaperone complex ensures stress granule integrity and dynamism, Mol. Cell 63 (5) (2016) 796–810.
[44] P. Kosuri, J. Alegre-Cebollada, J. Feng, A. Kaplan, A. Inglés-Prieto, C.L. Badilla, et al., Protein folding drives disulfide formation, Cell 151 (4) (2012) 794–806.
[45] C. Wang, J. Yu, L. Huo, L. Wang, W. Feng, C.C. Wang, Human protein-disulfide isomerase is a redox-regulated chaperone activated by oxidation of domain a', J. Biol. Chem. 287 (2) (2012) 1139–1149.
[46] C. Wang, W. Li, J. Ren, J. Fang, H. Ke, W. Gong, et al., Structural insights into the redox-regulated dynamic conformations of human protein disulfide isomerase, Antioxidants Redox Signal. 19 (1) (2013) 36–45.
[47] L. Wang, X. Wang, C.C. Wang, Protein disulfide-isomerase, a folding catalyst and a redox-regulated chaperone, Free Radic. Biol. Med. 83 (2015) 305–313.
[48] S. Parakh, J.D. Atkin, Novel roles for protein disulphide isomerase in disease states: a double edged sword? Front. Cell Dev. Biol. 3 (2015) 30.
[49] H. Li, K. Yang, W. Wang, Y. Niu, J. Li, Y. Dong, et al., Crystal and solution structures of human protein-disulfide isomerase-like protein of the testis (PDILT) provide insight into its chaperone activity, J. Biol. Chem. 293 (4) (2018) 1192–1202.
[50] T. Uehara, T. Nakamura, D. Yao, Z.Q. Shi, Z. Gu, Y. Ma, et al., S-nitrosylated protein-disulphide isomerase links protein misfolding to neurodegeneration, Nature 441 (7092) (2006) 513–517.
[51] A.K. Walker, M.A. Farg, C.R. Bye, C.A. McLean, M.K. Horne, J.D. Atkin, Protein disulphide isomerase protects against protein aggregation and is S-nitrosylated in amyotrophic lateral sclerosis, Brain 133 (1) (2010) 105–116.
[52] Y. Honjo, T. Horibe, A. Torisawa, H. Ito, A. Nakanishi, H. Mori, et al., Protein disulfide isomerase P5-immunopositive inclusions in patients with Alzheimer's disease, J. Alzheimers Dis. 38 (3) (2014) 601–609.

[53] C.I. Andreu, U. Woehlbier, M. Torres, C. Hetz, Protein disulfide isomerases in neurodegeneration: from disease mechanisms to biomedical applications, FEBS Lett. 586 (18) (2012) 2826–2834.
[54] A. Igbaria, P.I. Merksamer, A. Trusina, F. Tilahun, J.R. Johnson, O. Brandman, et al., Chaperone-mediated reflux of secretory proteins to the cytosol during endoplasmic reticulum stress, Proc. Natl. Acad. Sci. U. S. A. 116 (23) (2019) 11291–11298.
[55] K.E. Miller, Y. Kim, W.K. Huh, H.O. Park, Bimolecular fluorescence complementation (BiFC) analysis: advances and recent applications for genome-wide interaction studies, J. Mol. Biol. 427 (11) (2015) 2039–2055.
[56] H. Cho, F. Stanzione, A. Oak, G.H. Kim, S. Yerneni, L. Qi, et al., Intrinsic structural features of the human IRE1α transmembrane domain sense membrane lipid saturation, Cell Rep. 27 (1) (2019) 307–320.
[57] J. Chen, J.M. Gardner, Z. Yu, S.E. Smith, S. McKinney, B.D. Slaughter, et al., Yeast centrosome components form a noncanonical LINC complex at the nuclear envelope insertion site, J. Cell Biol. 218 (5) (2019) 1478–1490.
[58] L. Zhang, Y. Niu, L. Zhu, J. Fang, X. Wang, L. Wang, et al., Different interaction modes for protein-disulfide isomerase (PDI) as an efficient regulator and a specific substrate of endoplasmic reticulum oxidoreductin-1α (Ero1α), J. Biol. Chem. 289 (45) (2014) 31188–31199.
[59] X.L. Liu, J.Y. Hu, M.Y. Hu, Y. Zhang, Z.Y. Hong, X.Q. Cheng, et al., Sequence-dependent abnormal aggregation of human Tau fragment in an inducible cell model, Biochim. Biophys. Acta - Mol. Basis Dis. 1852 (8) (2015) 1561–1573.
[60] J.Y. Hu, D.L. Zhang, X.L. Liu, X.S. Li, X.Q. Cheng, J. Chen, et al., Pathological concentration of zinc dramatically accelerates abnormal aggregation of full-length human Tau and thereby significantly increases Tau toxicity in neuronal cells, Biochim. Biophys. Acta - Mol. Basis Dis. 1863 (2) (2017) 414–427.
[61] K.I. Lira-De León, P. Garćia-Gutiérrez, I.N. Serratos, M. Palomera-Cárdenas, M.del P. Figueroa-Corona, V. Campos-Peña, et al., Molecular mechanism of Tau aggregation induced by anionic and cationic dyes, J. Alzheimers Dis. 35 (2) (2013) 319–334.
[62] S. Mondragón-Rodríguez, G. Perry, J. Luna-Muñoz, M.C. Acevedo-Aquino, S. Williams, Phosphorylation of Tau protein at sites $Ser^{396-404}$ is one of the earliest events in Alzheimer's disease and Down syndrome, Neuropathol. Appl. Neurobiol. 40 (2) (2014) 121–135.
[63] M. Regalado-Reyes, D. Furcila, F. Hernández, J. Ávila, J. DeFelipe, G. León-Espinosa, Phospho-Tau changes in the human CA1 during Alzheimer's disease progression, J. Alzheimers Dis. 69 (1) (2019) 277–288.
[64] P. Momeni, A. Pittman, T. Lashley, J. Vandrovcova, E. Malzer, C. Luk, et al., Clinical and pathological features of an Alzheimer's disease patient with the MAPT ΔK280 mutation, Neurobiol. Aging 30 (3) (2009) 388–393.
[65] S.L. Shammas, G.A. Garcia, S. Kumar, M. Kjaergaard, M.H. Horrocks, N. Shivji, et al., A mechanistic model of Tau amyloid aggregation based on direct observation of oligomers, Nat. Commun. 6 (2015) 7025.
[66] F.J.A. Dennissen, M. Anglada-Huguet, A. Sydow, E. Mandelkow, E.M. Mandelkow, Adenosine A_1 receptor antagonist rolofylline alleviates axonopathy caused by human Tau ΔK280, Proc. Natl. Acad. Sci. U. S. A. 113 (41) (2016) 11597–11602.
[67] N. Mizushima, T. Yoshimori, B. Levine, Methods in mammalian autophagy research, Cell 140 (3) (2010) 313–326.
[68] D.J. Klionsky, K. Abdelmohsen, A. Abe, M.J. Abedin, H. Abeliovich, A.A. Arozena, et al., Guidelines for the use and interpretation of assays for monitoring autophagy (3rd edition), Autophagy 12 (1) (2016) 1–222.
[69] W.C. Xu, J.Z. Liang, C. Li, Z.X. He, H.Y. Yuan, B.Y. Huang, et al., Pathological hydrogen peroxide triggers the fibrillization of wild-type SOD1 via sulfenic acid modification of Cys-111, Cell Death Dis. 9 (2) (2018) 67.
[70] C. Riccardi, I. Nicoletti, Analysis of apoptosis by propidium iodide staining and flow cytometry, Nat. Protoc. 1 (3) (2006) 1458–1461.
[71] I. Vermes, C. Haanen, H. Steffens-Nakken, C. Reutelingsperger, A novel assay for apoptosis. Flow cytometric detection of phosphatidylserine expression on early apoptotic cells using fluorescein labelled Annexin V, J. Immunol. Methods 184 (1) (1995) 39–51.
[72] F. Du, Z. Zhou, Z.Y. Mo, J.Z. Shi, J. Chen, Y. Liang, Mixed macromolecular crowding accelerates the refolding of rabbit muscle creatine kinase: implications for protein folding in physiological environments, J. Mol. Biol. 264 (3) (2006) 469–482.
[73] E.M. Courchaine, A. Lu, K.M. Neugebauer, Droplet organelles? EMBO J. 35 (15) (2016) 1603–1612.
[74] T. Nakamura, S. Tu, M.W. Akhtar, C.R. Sunico, S. Okamoto, S.A. Lipton, Aberrant protein S-nitrosylation in neurodegenerative diseases, Neuron 78 (4) (2013) 596–614.
[75] T. Nakamura, O.A. Prikhodko, E. Pirie, S. Nagar, M.W. Akhtar, C.K. Oh, et al., Aberrant protein S-nitrosylation contributes to the pathophysiology of neurodegenerative diseases, Neurobiol. Dis. 84 (2015) 99–108.
[76] L. Mediani, J. Guillén-Boixet, J. Vinet, T.M. Franzmann, I. Bigi, D. Mateju, et al., Defective ribosomal products challenge nuclear function by impairing nuclear condensate dynamics and immobilizing ubiquitin, EMBO J. 38 (15) (2019) e101341.